TOPICAL REVIEW

Muon spin spectroscopy: magnetism, soft matter and the bridge between the two

L Nuccio[1], L Schulz[2,3], A J Drew[3,4]

[1] Department of Physics and FriMAT, University of Fribourg, Chemin du Musée 3, Fribourg CH-1700, Switzerland
[2] Microelectronics Research Center, The University of Texas at Austin, 10100 Burnet Road, Blg. 160 Austin, Texas 78758, USA
[3] Sichuan University, College of Physical Science & Technology, Chengdu 610064, Peoples Republic of China
[4] School of Physics and Astronomy, Queen Mary University of London, Mile End Road, London E1 4NS, UK

E-mail: A.J.Drew@scu.cn.edu or A.J.Drew@qmul.ac.uk

Abstract. The use of implanted muons to probe the spin dynamics and electronic excitations in a variety of magnetic and non-magnetic materials is reviewed and is split into three main sections, the first of which is an introduction to the historical context and background of the muon technique, which includes a basic introduction to the experimental method and underlying theoretical models. The second section is concerned with inorganic magnetic systems, starting with an overview of spin dynamics around critical points in ordered magnets. This is followed by an introduction to the early work on spin glasses, liquids and ices, which then continues onto the recent research in this area, including a discussion of some of the more controversial recent work on spin ices and magnetic monopoles. Information obtained by muons vital to two very important technological areas - magnetic semiconductors and next-generation energy materials - closes the discussion of inorganic magnetic materials. The final section is concerned with spin dynamics and magnetism in soft materials, and starts with discussing many of the key results in molecular magnets and organic spintronics. Spin dynamics in organic semiconductors, polymers and biological molecules is then covered, where contradictory experimental and theoretical work on charge carrier motion is presented. The similarities between the low-field relaxation rates in these "conducting" organic materials is compared to measurements of the electron spin relaxation measured in localised electronic states, obtained from high-field avoided level crossing spectroscopy in similar (and the same) materials.

1. Introduction and historical background

Since about the 1980s, muon beam techniques (collectively known as μSR - muon spin rotation, relaxation or resonance) have become increasingly important in condensed matter research. They have, for example, been used to study superconducting, magnetic and multiferroic materials, spatial and temporal magnetic disorder in systems like spin glasses and liquids, spin and charge carrier dynamics in organic semiconductors, defects in conventional semiconductors, Li diffusion rates in battery materials, chemical reaction rates and electron dynamics in biological molecules. The list is quite extensive, because of the fundamental and often unique information that μSR provides about the spin dynamics of the local environment in which the muon sits. Recent developments of the technique involve the production of a low-energy muon source, which has operated a fully-fledged user programme for a number of years now, and future developments include a high-field laser excitation facility. Perhaps even more exotically, a cosmic muon telescope has been successfully used to image the inside of volcanoes to try to predict when an eruption may occur [1], and more recently this technique has been used to image the internal structure of the Fukashima Daiichi reactors to assess the extent of the damage to the cores and knowledge of the location of the melted fuel [2].

While cosmic-ray muons could be used for spin spectroscopy *in principle*‡, if one had enough patience, the practical use of muon spectroscopy requires an intense beam of spin-polarised positive muons that are generated at government funded particle accelerators. There are currently no bench-top sources, although there has been some discussion of late that a non-scaling Fixed Field Alternating Gradient (FFAG) accelerator [3] may offer a relatively cheap solution that could be built and operated by a relatively well-endowed university (for a capital investment of the order of probably £10s million, instead of probably in excess of £1bn for a conventional source). Currently, four large-scale facilities are operational. The Paul Scherrer Institute (PSI) near Zurich and the TRIUMF Laboratory in Vancouver provide an intense quasi-continuous beam of muons. This makes them particularly suitable for low-energy muon techniques, which are highly inefficient (for example, 1 slow muon in every 10^5 fast muons), but because of the need to have one muon at a time in the sample, the useable flux on a typical spectrometer is limited (typically about 8 million events per hour). The ISIS Facility situated between Oxford and London and JPARC just north of Tokyo are pulsed sources that produce fewer muons on average than continuous sources, but have certain advantages and disadvantages to their timing structure, as discussed below. Several other muon sources (in the USA and former Soviet Union) are also historically important in developing the technique itself, as documented in a review by Patterson [4], but more recently the application of muons as probes of materials has prevailed.

Despite some of the rather exotic applications of μSR introduced above, being a rather unique and sensitive spin probe capable of measuring local magnetic fields, probably the two areas that the technique has had the most impact on are magnetism and superconductivity. Taking the former as an example, one of the most crucial measurements to characterise the behaviour of magnetic materials is the magnetisation itself. However, only when a material shows some long-range magnetic order resulting

‡ The cosmic ray muon telescope doesn't use the spin polarisation of the muon as a spectroscopic probe, but merely uses differences in absorption to map out an internal structure of a large km-sized object from a distance.

in a net magnetisation, for example a ferromagnet, will the net magnetisation be non-zero when there is no applied magnetic field. Dynamic or static disorder, in particular on the local level, may be present and important to measure. A conventional magnetometer essentially measures the magnetic moment per unit volume, averaged over the bulk of a sample, but this provides no information about the magnetisation at a local level. Moreover, magnetic disorder and spin dynamics make these bulk measurements particularly challenging. Whilst neutron scattering has offered great insight into dynamics, muons themselves offer unique and complimentary information, and are often applicable to materials whose properties are inaccessible by neutron techniques. As such, muon measurements of the local dynamic and quasi-static magnetic moments of are of crucial importance to understanding these materials.

Whilst the importance of muon measurements on magnetic materials is clear, the very same arguments can be made in a variety of materials that are not thought to be traditionally magnetic. This is because the muon technique is particularly sensitive to spin fluctuations, which are important in a whole host of materials, such as (organic and conventional) semiconductors, disordered spin systems and biologically active molecules. It is worth noting that as spin probe, it is not necessarily the dynamics of an electronic *spin* that are measured; it could also be the spatial dynamics of the electron that are probed. In this case, the measurements become possible as a result of the electron having a spin, but the spin itself is not the motivation behind the measurements. Many of these measurements are discussed in this review paper.

Over the years there have been many reviews and books about μSR (see e.g. [4, 5, 6, 7, 8, 9, 10]) that describe the principles and techniques of the spectroscopy comprehensively. Moreover, about a decade ago, a special issue with many articles about the applications of μSR was published [11, 12, 13, 14, 15, 16, 17, 18, 19, 20, 21, 22, 23, 24, 25, 26, 27, 28, 29, 30, 31]. Below, for completeness and convenience, we repeat some of this material that is relevant for the application of muons reviewed in this manuscript. Whilst muons have been extensively used in many materials classes, such as superconductors and conventional semiconductors, these areas are not the subject of this review as they have been extensively reviewed elsewhere (see for example [4, 12, 13, 14, 15, 26, 27, 28, 29, 32, 33, 34, 35, 36]). This review article focusses on two areas of application of the technique - magnetism and soft matter, with the underlying feature that brings the two together; electron spin dynamics. Indeed, it is the dynamic sensitivity of the probe that is arguably its most important feature.

2. The muon technique

2.1. Muon production and transport

Muons are spin $\frac{1}{2}$ leptons with a half-life $\tau_\mu = 2.19709(5)\mu$s, $\pm$ one electronic charge and a mass 105.65839(29) MeVc^2 [10]. It is worth noting, at the outset of this review, that it is possible to perform experiments with both negatively charged muons and positively charged anti-muons. When a negative muon is implanted into a solid, it is captured by an atom and cascades into the lowest muonic orbital. This is comparable with the radius of a heavy nucleus, so it would normally undergo nuclear capture. This results in complex behaviour beyond the scope of this review, which is concerned only with the use of positive muons, and we direct interested readers elsewhere [37]. The positively charged anti-muon, which within the μSR community is simply referred to

as a muon (dropping the "anti"), is the most extensively used variety of muons due to the possibility of using them as a probe of material properties. Indeed, from this point forward, we will continue with the (incorrect) convention of using the term "muon" for the positively charged variety, and limit this review exclusively to them.

The closest relatives of the μSR technique are the nuclear magnetic resonance (NMR) and the electron spin resonance (ESR) techniques. A detailed description of NMR and ESR can be found elsewhere (for example in [38]). In general, all three techniques are complementary to each other, although all are not always applicable or useful to study a particular material. There are numerous reasons to perform μSR experiments:

(i) μSR can be used to study materials in zero magnetic field.

(ii) It requires neither a local paramagnetic probe (ESR) nor a nuclear spin (NMR).

(iii) Muons can mimic hydrogen atoms and their chemical behaviour.

(iv) It is possible to create unbound or unpaired electrons to investigate otherwise neutral materials.

(v) An external probe field (RF-field) is not needed to penetrate the sample. This can be a big problem in the other two resonant techniques, for example, in superconductors where the penetration depth of the RF-radiation changes drastically at the superconductor transition.

However, there are clearly some disadvantages, such as a somewhat limited time window (up to a few tens of microseconds, for example), the need for a rather large and expensive particle accelerator, significant difficulties in identifying the site where the muon stops and certain limitations to the sample environment (e.g an upper limit to the magnetic field).

In order to create muons, protons are accelerated by large-sale particle accelerators and directed towards a graphite production target. As mentioned above, there are four main muon facilities in the world. Taking PSI as an example of a quasi-continuous source, the protons are accelerated to 590 MeV by a ring cyclotron and then guided to the pyrolytic graphite target, which is either 5 cm thick (target M) or 4 cm thick (target E) and can be changed depending on the needed mode of operation of the facility. Using ISIS as an example of a pulsed source, protons are accelerated by an 800 MeV synchrotron operating at 50 Hz with a double pulse structure (two pulses of 70 ns, separated by a few hundred ns). The protons are directed to a 7 mm thick pyrolytic graphite at a 45mm angle to the proton beam (resulting in an effective length of 10 mm). Once the protons are within the graphite target, they interact with other protons and neutrons to produce pions, which then decay with a half life of 26.030(23) ns [10] via the weak interaction into muons and neutrinos. Since the pion decays into two bodies, if it decays at rest, in order to conserve momentum the muon and neutrino are emitted in an opposite direction with well-defined momentums. The spin of the muon is also well-defined, since the pion has spin zero and the neutrino spin is always opposite to the direction of its momentum, as shown in Figure 1. Thus, the decay of positive pions at rest produces 100% longitudinally polarised positive muons.

In the muon experiments covered by this review, 100% spin polarised positively charged surface muons are transported from the production target and implanted into a sample. They are directed by a series of focussing and steering magnets that are configured in such a way to maintain spin polarisation of the muons. Having an energy of 4.119 MeV, surface muons penetrate between 0.1 to 1 mm depending mainly on

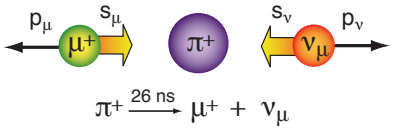

Figure 1: The pion (π^+) decays into a muon neutrino (ν_μ) and positively charged muon (μ^+). If the pion is at rest, then the muon and neutrino are emitted in opposite directions, resulting in the muon having 100% spin polarisation at production.

the mass density of the sample. Once inside the sample, the muon's kinetic energy is initially reduced to a few keV by inelastic scattering involving the Coulomb interaction, implying atomic excitation and ionisation. Typically lasting hundreds of picoseconds, this ionisation process leaves behind what are commonly termed "track electrons". The next stage of thermalisation is a process where the muons continuously "catch" and "lose" electrons, temporally forming neutral muonium atoms. During this process the muons diminish their energy typically to a few hundred eV within a picosecond. The final stage of the thermalisation is constituted by collisions between the muonium and atoms/molecules in the sample. In this process, the muonium might dissociate into a charged, unbound muon. For example, in metals a bare muon is the stable state. In other materials, such as semiconductors, the muonium remains. Importantly, there is an overall change of the spin direction of the muon ensemble of less than 15 mrad [6] for the entire thermalisation process. Therefore in practice the muon spin polarisation is preserved.

Muons decay via the weak interaction into a positron, muon-antineutrino and an electron-neutrino. The weak interaction breaks parity and relates the momentum of the emitted positron to the spin of the decaying muon. There is an asymmetry of the positron emission, and the direction depends on the orientation of the muon spin at the instance of the decay. The decay is a three body process, which leads to a distribution of positron energies, and thus the spatial emission distribution of the positrons, which is correlated with the orientation of the muon's spin. How the spatial emission distribution depends on the positron energy is shown in Figure 2a, and it takes the mathematical form [10]

$$dW(\epsilon,\theta) = \frac{e^{t/\tau_\mu}}{\tau_\mu}[1 + a(\epsilon)\cos\theta]n(\epsilon)d\epsilon d\cos\theta dt, \tag{1}$$

where $a(\epsilon) = (2\epsilon - 1)/(3 - 2\epsilon)$, $n(\epsilon) = 2\epsilon^2(3 - 2\epsilon)$ and the reduced positron energy ϵ is defined as $\epsilon = E/E_{max}$, where E_{max} is the maximum positron energy $E_{max} = 52.83$ MeV.

Thus, by placing an array of detectors around the sample environment that are capable of detecting the positron emission direction (e.g scintillators with photomultiplier tubes or solid state detectors such as avalanche photodiodes), it is possible to track the evolution of the muon's spin as a function of time.

In this review, the convention that the initial spin direction of the muon points towards the back detector and the momentum vector of the incident muon towards the front detector is used, as illustrated in Figure 2b. The number of events, N, as a function of time measured with the front (F) and back (B) detectors are given by:

$$N_B(t) = b_B + N_B^0 \exp(-t/\tau_\mu)[1 + A_0 P(t)] \tag{2}$$

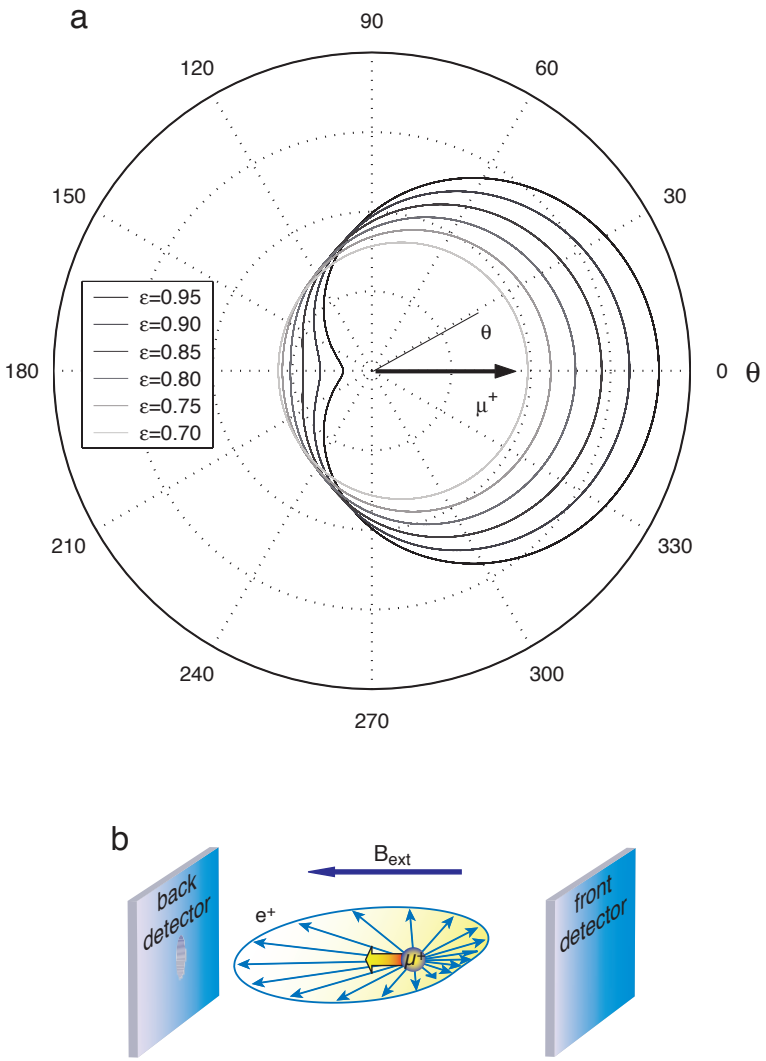

Figure 2: a) Polar plot of positron emission probability as a function of reduced positron energy, ϵ. b) Detector arrangement of a typical experiment, with the field applied in a longitudinal geometry.

and

$$N_F(t) = b_F + N_F^0 \exp(-t/\tau_\mu)[1 - A_0 P(t)] \tag{3}$$

where $P(t)$ is the polarisation of the muon's spin, A_0 is the initial asymmetry determined by the distribution of positron energies (thus angles) and detector geometry and is different for every spectrometer, N^0 is the initial number of events recorded and b is the background emanating from cosmic muons and other sources, such as electronic noise. In the case of vanishingly small background, the experimental

asymmetry that is often plotted in publications, is defined as

$$A(t) = \frac{N_B(t) - \alpha N_F(t)}{N_B(t) + \alpha N_F(t)} \tag{4}$$

where α is the detector efficiency, determined by many factors, including detector geometry, sample position, the amount of material surrounding the sample etc. α is different for every experiment performed as it is geometry dependent, but luckily easily estimated. When background and detector efficiency are removed, almost all information one would want to obtain about the muon's spin polarisation can be obtained from the forward-backward asymmetry function §:

$$A(t) = A_0 P(t). \tag{5}$$

The spins of unbound positive muons that implanted into a sample precess at the Larmor frequency $\omega_\mu = \gamma_\mu B$ in the presence of a magnetic field B, which is the vector sum of the applied field and any local field due to the magnetism or hyperfine fields present in the sample. The muon gyromagnetic ratio is $\gamma_\mu/2\pi$=135.534(5) MHzT^{-1} [7]. Therefore, by monitoring $P(t)$ it is possible to measure the internal magnetic field at the muon stopping site, the level of magnetic disorder (static or dynamic) and track changes in the magnetism as a function of an experimental variable, such as temperature.

The simplest time differential μSR technique is transverse field (TF) muon spin rotation, where the magnetic field is applied transverse to the initial muon polarisation. Depolarisation due to irreversible processes, such as muon diffusion and muon spin flipping due to hyperfine (HF) interaction with electrons and nuclei, is referred to as muon spin relaxation and is usually performed in a longitudinal field (LF) or zero field (ZF). It is also very common to investigate how the magnetism evolves in magnetic materials using ZF and LF techniques, the former often resulting in the muons spin precessing around the intrinsic long range order of the magnetism found in many materials.

On a final note, the nature of the production source has some important implications on the types of experiments that can be performed. At the quasi-continuous sources, the spectrometers typically operate with one muon in the sample at any given time‖. This is because the timers are started when a muon is detected entering the sample, and stopped when a positron event occurs. If two muons are present at the same time, but with different arrival times, how does one know which detected positron corresponds to which muon? The restriction of one muon at a time therefore significantly limits the flux of the instruments. The time resolution of a typical instrument is in the 100's ps regime, since the main limitation is the accuracy that the electronics of the instrument can measure time. In the case of a pulsed source, the time resolution is essentially determined by the proton pulse width convoluted with an exponential corresponding to the pion decay. At ISIS, the time resolution is a little less than 100 ns, which limits the sensitivity to high frequencies or fast relaxations. However, the limitation of knowing which positron corresponds to which muon is lifted, since the start time is determined by the pulse timing rather than

§ although there are more sophisticated ways to analyse data, which can yield more complex information about the muon's environment

‖ with the exception of a limited number of spectrometers sometimes used for Avoided Level Crossing measurements, which utilise a method known as "time integral counting" that only measures the time averaged counts on each detector

a particular muon entering the spectrometer. Several thousand muons can be present in the sample at any given time, meaning the useable flux is significantly higher than at the quasi-continuous sources, possibly by as much as a factor of 20 or 30.

2.2. Muon polarisation functions in magnetic materials

Many polarisation functions exist and the choice is depending on the exact nature of the system being studied and the muon's behaviour in it. Some complex materials systems result in relatively simple polarisation functions, others result in data that can be approximated by a simple combination of functions (and therefore trends can be extracted), and others require the use of advanced numerical methods to solve. Clearly, in a review article such as this, it is impossible to list them all, so we have only attempted to give a brief overview of the most important functions. A much more detailed discussion and derivation of many of the functions used can be found in ref. [8], for example.

In a magnetic material, the local magnetic field originates from a dipolar interaction with surrounding electronic or nuclear spins (plus any contact hyperfine interaction). The internal field due to long-range order (in ferro- or antiferro-magnets) often results in a local field with unique magnitude and direction for a given muon site. In a single crystal and for a single muon stopping site, the muons' spin then precesses as

$$P(t) = \cos^2\theta + \sin^2\theta\cos(\omega_\mu t) \tag{6}$$

where θ is the angle between the internal field experienced by the muon and the muon's spin polarisation. The average polarisation for a given θ, calculated from the time spectra, is shown in Figure 3. Clearly, in a single crystal, the value of θ determines both the amplitude and the baseline of the precessing signal, and this is material and muon site dependent. In a polycrystalline magnetic material, however, the differently oriented grains means one must take an average over θ, resulting in a 1/3 non-relaxing baseline and 2/3 precessing signal for randomly oriented grains

$$P(t) = \frac{1}{3} + \frac{2}{3}\cos(\omega_\mu t). \tag{7}$$

For the case of a polycrystalline sample with some degree of preferred crystallographic orientation, the relative weights of the oscillating and non-oscillating signal would often be modified, analogous to the case of a single crystal.

For the case where there is a distribution of fields at the muon site, for example due to magnetic or crystallographic disorder, then the precession signal becomes damped. The form of this damping depends on the nature of the disorder. Either a Gaussian or exponential envelope is relatively common.

When the direction of surrounding magnetic moments is random, such is the case for nuclear dipolar fields or the randomly frozen electronic spins, then the local fields that the muon ensemble experiences are a continuous distribution. Nuclear dipolar fields often originate from several static moments, with a random orientation, each a similar distance from the muon site. The vector sum of the fields from these nuclear moments, or similarly arranged electronic spins, often results in an approximate Gaussian distribution of local fields. Integrating over the local field results in the famed Kubo-Toyabe function [39]

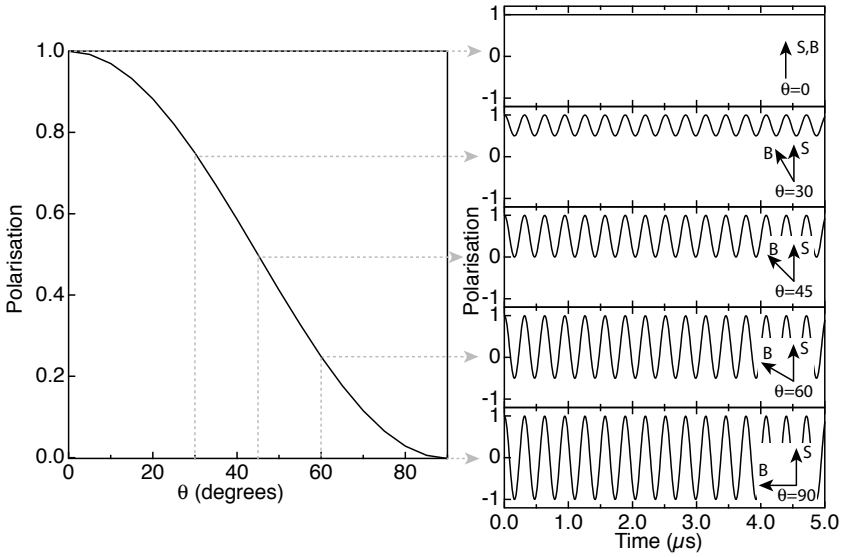

Figure 3: A calculation of the polarisation in a magnetic material as a function of angle between the muon spin, S, and the internal magnetic field at the muon site, B.

$$P(t) = \frac{1}{3} + \frac{2}{3}\left(1 - \gamma_\mu^2 \Delta_G^2 t^2\right) e^{\left(-\frac{\gamma_\mu^2 \Delta_G^2 t^2}{2}\right)}. \tag{8}$$

As can be seen in Figure 4, the Kubo-Toyabe function in zero field is an underdamped oscillation (a single localised minimum) with a period corresponding approximately to the maximum probability in the field distribution. In a longitudinally applied field, the Kubo-Toyabe function takes the form [40]

$$P(t) = 1 - \frac{2\Delta_G^2}{B^2}\left[1 - \cos\left(\gamma_\mu B t\right) e^{\left(-\frac{\gamma_\mu^2 \Delta_G^2 t^2}{2}\right)}\right] + \frac{\gamma_\mu \Delta_G^4}{B^3}\int_0^t \sin\left(\gamma_\mu B \tau\right) e^{\left(-\frac{\gamma_\mu^2 \Delta_G^2 \tau^2}{2}\right)} d\tau. \tag{9}$$

This is plotted for various longitudinal fields in Figure 4, where it can be seen that the external field decouples the muon's spin from the internal field when they become comparable to each other. Indeed, confirming whether the decoupling field corresponds to the oscillation frequency is a good check for spin dynamics.

So far we have assumed that the muon is at rest in the material under study and the magnetic moments that give rise to the field distribution being measured is static. A common method for measuring the spin fluctuation rate of field distribution is to measure the LF dependence of the muon relaxation rate. In the fast-fluctuation limit, the muon spin relaxation function in ZF is an exponential [41] where the damping rate is inversely proportional to the internal field correlation frequency (or proportional to the field correlation time). When a LF is applied, the exponential damping rate, λ, varies as

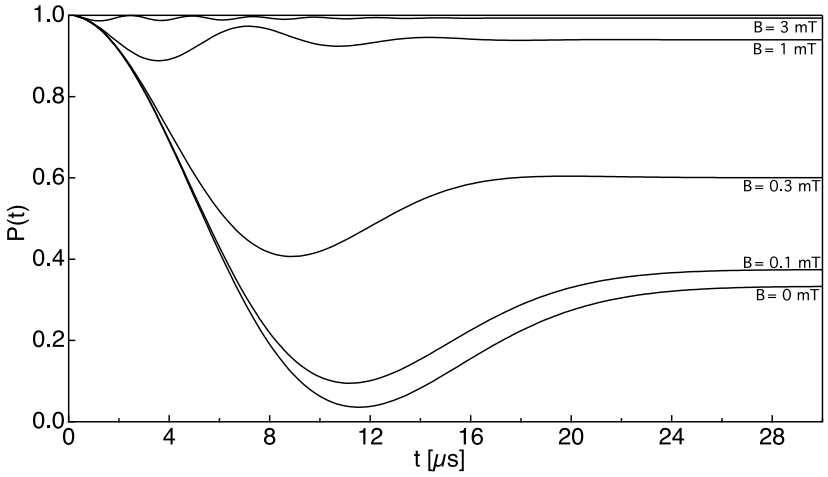

Figure 4: The Kubo-Toyabe function plotted for several different LFs, for $\gamma_\mu \Delta_G = 0.15$ MHz.

$$\lambda \propto \frac{1}{\omega_\mu^2 + \nu_B^2} \tag{10}$$

where ν_B is the internal field correlation frequency. In many materials, by applying an external LF, one is therefore able to tell the difference between small static moments or larger dynamic moments. Further details on this can be found elsewhere (see for example [8, 10, 42]).

A stretched exponential relaxation function is sometimes observed in experimental data, which takes the form

$$P(t) = \exp(-\lambda t^\beta) \tag{11}$$

where β is the stretch parameter. There are only limited circumstances where a stretched exponential relaxation function has a deep physical meaning. Indeed, a superposition of a small number of exponentials (corresponding to different muon sites, for example) can be observed as a stretched exponential relaxation. As can be seen from Figure 5a, a stretched exponential can be extremely similar to a superposition of exponentials (three in this case) when plotted on a linear scale. However, by plotting $-t/\ln(P(t))$ as shown in Figure 5b, the difference becomes very clear indeed [43]. A good example of a true stretched exponential function being present is the spin glass, which is covered in detail later in this article. The stretched-exponential form in these systems could either be related to the spatial averaging of many different exponential decays (there is a spatial distribution of both the magnetic moments sampled by the muons and the spin fluctuation rate of each moment), or the non-Markovian dynamics of the moments.

2.3. Muonium and ALCs

In the case of semiconductors, dielectrics, and molecular compounds, a large fraction of muons are often found in a stable bound state with an electron, i.e. the so-called

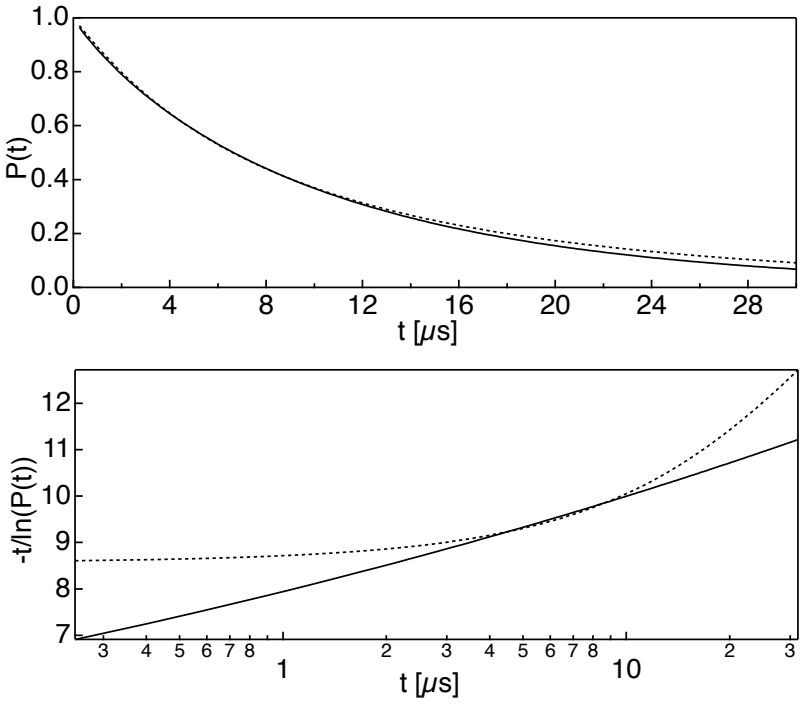

Figure 5: (a) A stretched exponential function with β=0.9 and λ=0.1 MHz (solid line) compared to a superposition of three exponentials (with equal weighting), with λ = 0.05, 0.1 and 0.2 MHz (dashed line). It is extremely challenging to tell the difference between the two, with the most difference being at very high times, where there is often considerable scatter of experimental data. (b) The same data replotted, with $-t/\ln(P(t))$ on the y -axis. The difference is very clear, and is readily observable in experimental data, even with relatively low counting statistics.

muonium atom is observed. This is because the Debye screening length is quite long. The muon and electron spins are coupled by the hyperfine interaction, which can be either isotropic or anisotropic. In an organic sample, the muonium can form a bond with the molecules in the last step of the thermalisation process, joining a molecule at a site with high electron concentration, such as unsaturated bonds or aromatic rings. Muonium that sits unbound in interstitial sites is often referred to as "vacuum muonium", whereas when muonium has reacted with a molecule to form a paramagnetic molecule, the resulting complex is known as a muoniated radical. The value of the isotropic muon-electron HF constant is determined by the overlap of the muon and electron wavefunctions, via the Fermi contact interaction. The muon's wavefunction is essentially a delta-function, whereas in muoniated radicals, the electron's wavefunction is spread over a large portion of the molecule. The degree of localisation of the electron's wavefunction, where it is centred with respect to the muon and the electron's orbital angular momentum determine the value of the HF constant to the muon, and this varies considerably between different muon adduct sites, even ones that are next to each other on the same molecule. As a consequence, the hyperfine

coupling constant strongly varies between sites, but is readily calculable using, for example, density functional theory (DFT). In addition to a change in the isotropic hyperfine coupling constant, there can also be an anisotropic hyperfine interaction between the muon and electron. This is averaged out to zero when the reorientation rate of the molecule is much larger than the dipolar part of the HF coupling, normally the case with a liquid, but anisotropic coupling is generally present for muoniated radicals in solids.

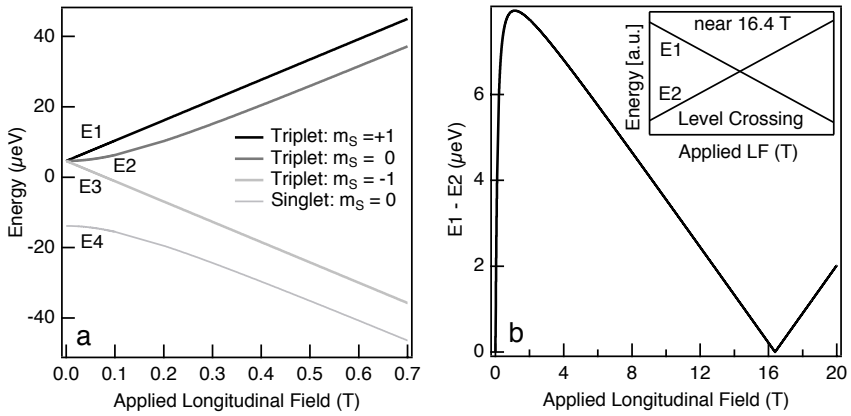

Figure 6: a) Breit-Rabi diagram of an isolated isotropic muonium in a longitudinal magnetic field. In zero-field the triplet states are degenerate and at a higher energy than the singlet state. The degeneracy of the triplet states is lifted in the magnetic field. b) The energetic difference between the triplet states $m_{\mathrm{S}} = +1$ and $m_{\mathrm{S}} = 0$ is shown. The energy levels E_1 and E_2 cross at about 16.4 T. The inset illustrates the energy level crossing.

Isolated isotropic muonium serves as a simple example to demonstrate the principal effects of the interaction between the electron spin, $\vec{S_{\mathrm{e}}}$, and the muon spin, $\vec{S_{\mu}}$, in an external magnetic field. The HF coupling vacuum muonium is solely described by the isotropic HF interaction, with a coupling constant $A = 4.46$ GHz, since it has a spherical electron distribution around the muon, analogous to hydrogen. To account for the interaction between the electron spin, muon spin and the magnetic field, $\vec{B}$, the Zeeman terms are needed in the Hamiltonian [9]

$$H_0 = -\gamma_{\mu}\vec{S}_{\mu} \cdot \vec{B} + \gamma_{\mathrm{e}}\vec{S}_{\mathrm{e}} \cdot \vec{B} + A\vec{S}_{\mu} \cdot \vec{S}_{\mathrm{e}}. \tag{12}$$

The spins are defined by the Pauli spin matrices, which are used to calculate the energy levels of the coupled two-spin system. The energy eigenvalues are given by [9]

$$E_1 = \frac{\hbar}{4}\left[A + 2B\left(\gamma_{\mathrm{e}} - \gamma_{\mu}\right)\right] \tag{13}$$

$$E_2 = -\frac{\hbar}{4}\left[A - 2\sqrt{A^2 + B^2\left(\gamma_{\mathrm{e}} + \gamma_{\mu}\right)^2}\right] \tag{14}$$

$$E_3 = \frac{\hbar}{4}\left[A - 2B\left(\gamma_{\mathrm{e}} - \gamma_{\mu}\right)\right] \tag{15}$$

$$E_4 = -\frac{\hbar}{4}\left[A + 2\sqrt{A^2 + B^2\left(\gamma_\mathrm{e} + \gamma_\mu\right)^2}\right]. \tag{16}$$

Figure 6a shows the behaviour of the energy levels at low (<1 T) external magnetic fields. The two-spin system exists either as a triplet (E_1-E_3) or as a singlet (E_4) state. The degeneracy of the triplet states is lifted by the external magnetic field via the Zeeman interaction. For vacuum muonium, the energy levels E_1 and E_2 intersect at about 16.4 T (corresponding A = 4.46 GHz) as can be seen in the main graph of Figure 6b, where the difference of E_1 and E_2 vanishes. The inset of the same figure illustrates this crossing, which will be dealt with later in this section.

One can use the product of the spin up and down vectors of the muon and the electron to define the eigenvectors of this coupled spin system [9]

$$\mid \Psi_1\rangle = |\uparrow_\mu\uparrow_\mathrm{e}\rangle \tag{17}$$

$$\mid \Psi_2\rangle = c_1\,|\uparrow_\mu\downarrow_\mathrm{e}\rangle + c_2\,|\downarrow_\mu\uparrow_\mathrm{e}\rangle \tag{18}$$

$$\mid \Psi_3\rangle = |\downarrow_\mu\downarrow_\mathrm{e}\rangle \tag{19}$$

$$\mid \Psi_4\rangle = c_2\,|\uparrow_\mu\downarrow_\mathrm{e}\rangle - c_1\,|\downarrow_\mu\uparrow_\mathrm{e}\rangle, \tag{20}$$

where the prefactors are given by

$$c_1 = \frac{1}{\sqrt{2}}\sqrt{1 - \frac{B}{\sqrt{B_0^2 + B^2}}} \tag{21}$$

and

$$c_2 = \frac{1}{\sqrt{2}}\sqrt{1 + \frac{B}{\sqrt{B_0^2 + B^2}}}. \tag{22}$$

where $B_0 = A/\left(\gamma_\mu + \gamma_\mathrm{e}\right)$. Since the incoming 100% spin-polarised muons are coupled to unpolarised electrons, the spin system can initially be either in the $|\uparrow_\mu\uparrow_\mathrm{e}\rangle$ state (50%) or in the $|\uparrow_\mu\downarrow_\mathrm{e}\rangle$ state (50%). The former corresponds to the $\mid \Psi_1\rangle$ state (Equation 17). The latter is a combination of the states 18 and 20 [9].

The time evolution of the muon spin ensemble in the muonium state can be derived with the spin density matrix formalism as presented in [4]. At $t = 0$, the terms describing the electron polarisation and the mixed polarisations are zero. Thus, the spin density matrix is given by [4]

$$\rho(0) = \frac{1}{4}\left(1 + \vec{P}_\mu(0)\cdot\vec{\sigma}\right) \tag{23}$$

where $\vec{P}_\mu(t=0) = (0,0,1)$ is the initial muon spin polarisation. $\vec{\sigma}$ denotes the Pauli spin matrix of the muon spin. Equation 23 can be simplified, if B points into the z-direction. Now, only the polarisation of the muon spin along the z-direction shall be regarded. Equation 23 takes the following form:

$$\rho(0) = \frac{1}{4}\left(1 + \sigma_\mathrm{z}\right). \tag{24}$$

The application of the quantum mechanical equation of motion $i\hbar\mathrm{d}\rho/\mathrm{d}t = [H,\rho]$ provides the time- and field-dependent spin polarisation

$$P_\mu(t) = Tr\left[\left(\exp\left(\frac{-iHt}{\hbar}\right)\rho(0)\exp\left(\frac{iHt}{\hbar}\right)\right)\cdot\vec{\sigma}\right]. \tag{25}$$

Performing this calculation leads to the field-dependent time evolution of the muon spin polarisation [9, 4]

$$P_\mu(t) = \underbrace{\frac{A^2 + 2B^2\left(\gamma_\mathrm{e} + \gamma_\mu\right)^2}{2A^2 + 2B^2\left(\gamma_\mathrm{e} + \gamma_\mu\right)^2}}_{\mathrm{Non-oscillatory\ part}} + \underbrace{\frac{A^2}{2A^2 + 2B^2\left(\gamma_\mathrm{e} + \gamma_\mu\right)^2}\cos\left(\omega_{24}t\right)}_{\mathrm{Oscillatory\ part}} \tag{26}$$

$$= \overline{P}_{\mu,iso} + P_\mathrm{osc}. \tag{27}$$

The polarisation function, $P_\mu(t)$, consists of two parts: the non-oscillatory part, $\overline{P}_{\mu,iso}$, the so-called repolarisation curve, and the oscillatory component, P_osc, the so-called Rabi oscillation. The spin polarisation of the muon ensemble oscillates at a frequency of $\omega_{24} = \sqrt{A^2 + B^2\left(\gamma_\mathrm{e} + \gamma_\mu\right)^2}$ which corresponds to the energy difference of E_2 and E_4.

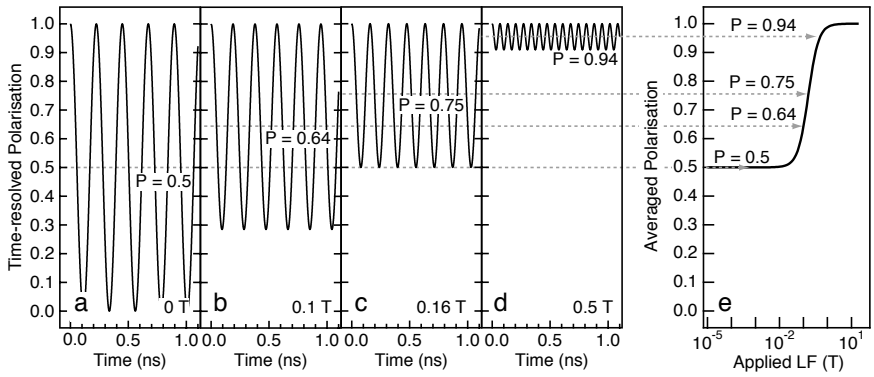

Figure 7: a-d) Breit-Rabi oscillation at $B = 0$ T, 0.1 T, 0.1585 T and 0.5 T for isotropic vacuum muonium. e) Corresponding repolarisation curve (see text).

Figure 7a shows that the polarisation at $B = 0$ oscillates between 0 and 1. This arises from the superposition of the non-oscillatory polarisation of 0.5 from the $|\uparrow_\mu\uparrow_\mathrm{e}\rangle$ state and the component that oscillates between +0.5 and -0.5 originating from the $|\uparrow_\mu\downarrow_\mathrm{e}\rangle$ state. An external magnetic field modifies the state $|\uparrow_\mu\downarrow_\mathrm{e}\rangle$, because the prefactors c_1 and c_2 (Equ. 21 and 22) are field-dependent. The Figures 7b-d demonstrate how the amplitude reduces and the oscillation frequency increases as the energetic distance between E_2 and E_4 widens in the magnetic field (c.f. Figure 6a). In Figure 7c the external magnetic field $B = 0.1585$ T (Figure 7d) matches the HF coupling strength of 4.46 GHz. In the limit of very high magnetic fields, the oscillation amplitude vanishes as $c_1 \to 0$ and $c_2 \to 1$ [9].

The Rabi oscillations are usually very fast and can often not be resolved in experiments, so one measures the time-averaged spin polarisation of the muon ensemble, which is given by [44]:

$$\overline{P_\mu} = \frac{\int_0^\infty P_\mu(t)\mathrm{e}^{-\lambda t}\mathrm{d}t}{\int_0^\infty \mathrm{e}^{-\lambda t}\mathrm{d}t}. \tag{28}$$

By substituting Equation 27 into 28 one obtains the repolarisation function for a

coupled isotropic two-spin system [45]:

$$\overline{P}_{\mu,iso} = \frac{A^2 + 2B^2\left(\gamma_\mathrm{e} + \gamma_\mu\right)^2}{2A^2 + 2B^2\left(\gamma_\mathrm{e} + \gamma_\mu\right)^2}. \tag{29}$$

The repolarisation curve embodies the time-average of the oscillations as illustrated by the arrows in Figure 7. The repolarisation of the muon spin ensemble is shown in Figure 7e. The spin polarisation is regained in the external magnetic field from 0.5 at low fields to 1 at fields above 10 T. Clearly, for muoniated radicals this magnetic field is significantly reduced, as it depends on the HF coupling constant (which is significantly reduced for muoniated radicals).

In the case of a non-spherical electron distribution with either an axial symmetry or full anisotropy, the so-called anisotropic HF interaction is present. For axial symmetry the anisotropic hyperfine coupling parameter $D_\perp$ is introduced and the repolarisation curve changes to [45]

$$\overline{P}_{\mu,axial} = \frac{\frac{1}{2}A^2\left[\langle\cos^2\phi\rangle D_\perp^2 + B^2\left(\gamma_\mathrm{e} - \gamma_\mu\right)^2\right] + B^2\left(\gamma_\mathrm{e} + \gamma_\mu\right)^2\left[D_\perp^2 + B^2\left(\gamma_\mathrm{e} - \gamma_\mu\right)^2\right]}{\left[A^2 + B^2\left(\gamma_\mathrm{e} + \gamma_\mu\right)^2\right]\cdot\left[D_\perp^2 + B^2\left(\gamma_\mathrm{e} - \gamma_\mu\right)^2\right]}. \tag{30}$$

where $\langle\cos^2\phi\rangle \approx 1/3$ corresponds to the powder average.

In the case of a fully anisotropically coupled spin system, the principle axes of the hyperfine coupling tensor $\widetilde{A}$ are defined as A_x=$A-D_1/2-D_2/2$, A_y=$A-D_1/2+D_2/2$ and A_z=$A-D_1$ [45]. The dipolar parameters D_1 and D_2 describe the anisotropy of the system. The repolarisation curve is then approximated by [45]

$$\overline{P}_{\mu,full} = \frac{1}{6}\left[\frac{\left(\gamma_\mathrm{e} - \gamma_\mu\right)^2 B^2}{\frac{5}{12}D_2^2 + \left(\gamma_\mathrm{e} - \gamma_\mu\right)^2 B^2}\right] + \frac{1}{3}\left[\frac{\left(\gamma_\mathrm{e} - \gamma_\mu\right)^2 B^2}{\frac{15}{16}D_1^2 + \left(\gamma_\mathrm{e} - \gamma_\mu\right)^2 B^2}\right] + \frac{1}{2}\left[\frac{\left(\gamma_\mathrm{e} + \gamma_\mu\right)^2 B^2}{A^2 + \left(\gamma_\mathrm{e} + \gamma_\mu\right)^2 B^2}\right]. \tag{31}$$

In an organic material, there are often several muonium sites. Each muonium site gives rise to an individual repolarisation curve. Thus, a linear combination of the equations 29, 30 and 31 can be used to fit the repolarisation data, however this does not result in a particularly accurate estimate of the hyperfine coupling constants and a better way to extract them is to directly measure the loss in polarisation at an avoided level crossing (ALC) [46, 47], or to perform transversal field μSR in the Paschen-Back limit [4, 8, 46].

In addition to the anisotropy we must take into account one additional spin-1/2 nuclei. Other nuclear spins and high-order interactions such as quadrupole and octupole interactions are omitted to simplify the equations and to diminish the number of indices and summations. Furthermore, for simplicity only systems that can be described with an axial hyperfine symmetry shall be considered. The Hamiltonian $H = H_0 + H_{\mu,\mathrm{aniso}} + H_\mathrm{nuclei}$ of this three-spin system for axial symmetry is defined as follows [10]

$$H_0 = -\gamma_\mu\vec{S}_\mu\cdot\vec{B} + \gamma_\mathrm{e}\vec{S}_\mathrm{e}\cdot\vec{B} + A\vec{S}_\mu\cdot\vec{S}_\mathrm{e} \tag{32}$$

$$H_{\mu,\mathrm{aniso}} = \frac{1}{2}A_\mu \left(S_\mathrm{e}^+ S_\mu^- + S_\mathrm{e}^- S_\mu^+\right) - D_{\mu,\perp}\Bigg[\left(1-3\cos^2\theta\right) S_\mathrm{e} S_\mu \tag{33}$$

$$- \frac{1}{4}\left(1-3\cos^2\theta\right)\left(S_\mathrm{e}^+ S_\mu^- + S_\mathrm{e}^- S_\mu^+\right) \qquad \Delta M = 0 \tag{34}$$

$$- \frac{3}{2}\left(\sin\theta\cos\theta\exp(-i\phi)\right)\left(S_\mathrm{e} S_\mu^+ + S_\mathrm{e}^+ S_\mu\right) \quad \Delta M = 1 \tag{35}$$

$$- \frac{3}{2}\left(\sin\theta\cos\theta\exp(+i\phi)\right)\left(S_\mathrm{e} S_\mu^- + S_\mathrm{e}^- S_\mu\right) \quad \Delta M = 1 \tag{36}$$

$$- \frac{3}{4}\left(\sin^2\theta\exp(-2i\phi)\right)\left(S_\mathrm{e}^+ S_\mu^+\right) \qquad \Delta M = 2 \tag{37}$$

$$- \frac{3}{4}\left(\sin^2\theta\exp(+2i\phi)\right)\left(S_\mathrm{e}^- S_\mu^-\right)\Bigg] \qquad \Delta M = 2 \tag{38}$$

$$H_{\mathrm{nuclei}} = \underbrace{\sum_{\mathrm{k}=1}^{\mathrm{n}} -\gamma_\mathrm{k} I_\mathrm{k}\cdot B_\mathrm{z}}_{\text{Zeeman term}} + \frac{1}{2}\sum_{\mathrm{k}=1}^{\mathrm{n}} A_\mathrm{k}\left(S_\mathrm{e}^+ I_\mathrm{k}^- + S_\mathrm{e}^- I_\mathrm{k}^+\right) \tag{39}$$

$$- \sum_{\mathrm{k}=1}^{\mathrm{n}} D_{\mathrm{k},\perp}\Bigg[\left(1-3\cos^2\theta\right) S_\mathrm{e} I_\mathrm{k} \tag{40}$$

$$- \frac{1}{4}\left(1-3\cos^2\theta\right)\left(S_\mathrm{e}^+ I_\mathrm{k}^- + S_\mathrm{e}^- I_\mathrm{k}^+\right) \qquad \Delta M = 0 \tag{41}$$

$$- \frac{3}{2}\left(\sin\theta\cos\theta\exp(-i\phi)\right)\left(S_\mathrm{e} I_\mathrm{k}^+ + S_\mathrm{e}^+ I_\mathrm{k}\right) \quad \Delta M = 1 \tag{42}$$

$$- \frac{3}{2}\left(\sin\theta\cos\theta\exp(+i\phi)\right)\left(S_\mathrm{e} I_\mathrm{k}^- + S_\mathrm{e}^- I_\mathrm{k}\right) \quad \Delta M = 1 \tag{43}$$

$$- \frac{3}{4}\left(\sin^2\theta\exp(-2i\phi)\right)\left(S_\mathrm{e}^+ I_\mathrm{k}^+\right) \qquad \Delta M = 2 \tag{44}$$

$$- \frac{3}{4}\left(\sin^2\theta\exp(+2i\phi)\right)\left(S_\mathrm{e}^- I_\mathrm{k}^-\right)\Bigg]. \qquad \Delta M = 2 \tag{45}$$

The angle between magnetic field, B, and the symmetry axis is denoted as θ. ϕ is the azimuthal angle [48]. Without loss of generality, B has been assumed to be parallel to the z-axis. The isotropic and dipolar HF coupling constants describing the HF interaction between the nuclear spin k and the electron spin are denoted as A_k and $D_{\mathrm{k},\perp}$. S_e, I_k and S_μ are the z-component of the spin operators. $S_\mathrm{e}^\pm$, $I_\mathrm{k}^\pm$, $S_\mu^\pm$ denote the lowering (-) and raising (+) operators. ΔM is the change of the total magnetic spin quantum number $M = m_\mathrm{e} + m_\mu + m_\mathrm{k}$ of the coupled spin system. The magnetic dipole interaction of the muon and nuclear point-dipole with the unpaired electron can be described in this approximation by [48]

$$D_{\mu,\mathrm{k},\perp} = -\frac{\gamma_\mathrm{e}\gamma_{\mu,\mathrm{k}}\hbar}{2\pi}\left\langle\frac{1}{r^3}\right\rangle. \tag{46}$$

The additional terms $H_{\mu,\mathrm{aniso}}$ and H_{nuclei} give rise to four main modifications as compared to the isolated, isotropic muonium:

(i) The number of energy eigenstates increases by a factor of 2^n, where n is the number of spin 1/2 nuclei. For instance, by including one additional nuclear spin to the electron-muon two-spin system, the number of eigenstates increases from four to eight.

(ii) The repolarisation function is altered as mentioned above.

(iii) The degeneracy of the triplet states at $B = 0$ is lifted.

(iv) Most importantly, the energy levels do not cross anymore, but establish so-called avoided level crossings.

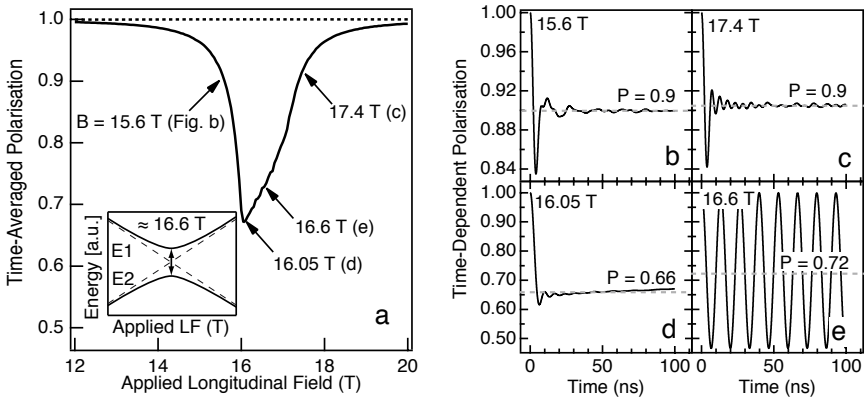

Figure 8: a) A comparison of the simulated muon spin polarisation of the isotropic (dashed line) and the anisotropic muonium (solid line) without nuclear spins. Inset: the two approaching energy levels no longer cross, resulting in a so-called avoided level crossing (ALC). b-e) The time-resolved oscillation at various fields near the ALC. Note the minima in the ALC does not correspond to the maximum oscillation amplitude. The powder average used for these simulations are the origin of the damping. It should be noted that it is not normal to have such a high isotropic HF coupling (4.46 GHz) and a non-zero anisotropic HF coupling.

As stated earlier, for an isotropic muonium the energy levels of the $m_{\mathrm{S}} = +1$ and $m_{\mathrm{S}} = 0$ triplet states cross near 16.4 T (corresponding to a muon-electron hyperfine coupling constant of 4.46 GHz). If the HF interaction of the muonium is anisotropic or additional nuclear spins interact with the spins of the muonium, the eigenstates involve a mixture of spin states. The former approximation of pure Zeeman product eigenstates near the energy levels crossing is then no longer valid. In fact, the energy levels do not intersect anymore, but "repel" each other in the crossover region; a so-called avoided level crossing of the energy levels develops. It is worth noting that in the experimental literature (and to some extent the theoretical literature too) it is common to refer to the loss of muon polarisation as a result of the avoided energy level crossing as an ALC resonance, or simply just ALC. An illustration of two energy states that exhibit the described behaviour is shown in the inset of Figure 8a. The previous crossing is indicated by the dashed lines.

The ALC resonance has an asymmetric shape due to the anisotropy of the HF interaction. The centre of the resonance is not exactly at the minimum of the ALC lineshape (16.05 T), but at a slightly higher field (16.6 T). The greater the difference between the two anisotropic HF coupling constants D_1 and D_2, the more pronounced the asymmetric shape of the ALC is. The mixture of the spin states enables a Rabi oscillation. The oscillation frequency corresponds again to the difference of the two energy levels E_1 and E_2. In the Figures 8b-e the time-resolved spectra are shown for the magnetic fields indicated in Figure 8a. The damping originates from the powder average used to calculate the ALC. For an ideal system (e.g. in a perfect single crystal without dynamic processes) this damping would be absent.

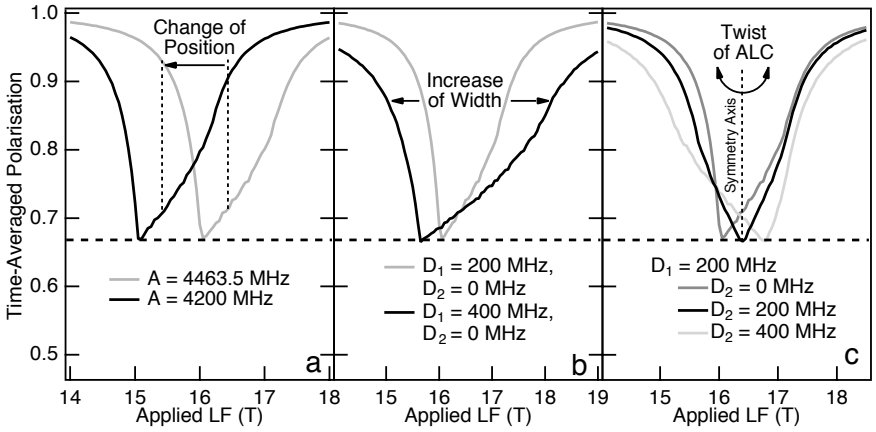

Figure 9: The impact of the HF coupling constants A, D_1 and D_2 on an ALC. a) Shift of the ALC position as a function of A. b) Changing D_1 alters the width of the ALC but leaves its position unaffected. c) A change of the relative strength of D_1 and D_2 causes a reshaping of the ALC without modificaton of the position.

Three types of ALCs shall be distinguished on the basis of a Hamiltonian with axial symmetry [49, 50, 51]. This distinction is also valid for a fully anisotropic system.

$\Delta M = 0$: The isotropic coupling of the muonium to a nuclear spin causes a so-called muon-nuclear spin flip-flop transition. The active terms of the Hamiltonian with axial symmetry are $A_\mathrm{k}\left(S_\mathrm{e}^+ I_\mathrm{k}^- + S_\mathrm{e}^- I_\mathrm{k}^+\right)$ and $A_\mu\left(S_\mathrm{e}^+ S_\mu^- + S_\mathrm{e}^- S_\mu^+\right)$. The resonance occurs in media with nuclear spins¶. It is of indirect nature, because the spin transfer from the muon to the nucleus is mediated by the electron. The resonance occurs at about

$$B_\mathrm{r}(\Delta_0) = \frac{|A_\mu - A_\mathrm{k}|}{2\left(\gamma_\mu - \gamma_\mathrm{k}\right)} - \frac{A_\mu + A_\mathrm{k}}{2\gamma_\mathrm{e}} \tag{47}$$

with effective HF coupling constants, A_i, which include any compensation needed for anisotropy [49]. These resonances are readily observed in the liquid state, and can have a FWHM as small as 2 mT. Despite being normally present, they are not always observable in the solid state.

$\Delta M = 1$: The most simple but very intense ALC involves a pure muon-electron spin-flip arising from the dipolar components of the HF interaction. This resonance

¶ Or other tertiary spins (e.g a secondary unpaired electron [85])

appears at the field

$$B_{\mathrm{r}}(\Delta_1) = \frac{|A_\mu|}{2\gamma_\mu} - \frac{A_\mu}{2\gamma_{\mathrm{e}}}. \tag{48}$$

It is usually only present in solid samples, because in liquids and gases the muonium experiences very fast reorientations that average out the dipolar terms [49]. These very intense and broad resonances can dwarf the $\Delta M = 0$ resonances in experiments [52].

$\Delta M = 2$: These very weak ALCs, caused by the so-called muon-nuclear spin flip-flip transitions, have no practical relevance for disordered systems. They are similar to the $\Delta M = 0$ resonance but are driven by the anisotropic parts of the Hamiltonian $S_{\mathrm{e}}^{+} I_{\mathrm{k}}^{+}$, $S_{\mathrm{e}}^{-} I_{\mathrm{k}}^{-}$, $S_{\mathrm{e}}^{+} S_{\mu}^{+}$ and $S_{\mathrm{e}}^{-} S_{\mu}^{-}$.

In Figure 9 the effect of the isotropic and anisotropic HF coupling constants A and D_{i} on a fully anisotropic ALC is demonstrated. The isotropic HF coupling constant, A, determines the position of the ALC. The parameters D_{i} define its width and shape. In addition, reorientational dynamics, like rotations or vibrations of the muon site, can alter the line shape due to averaging effects [49, 53].

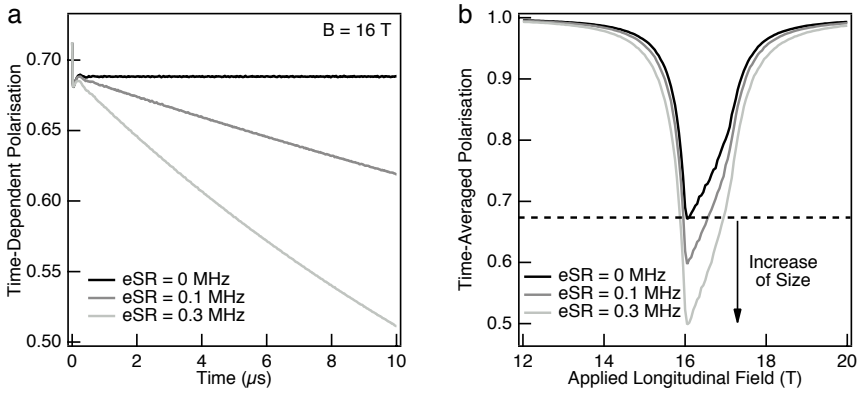

Figure 10: The influence of dynamical effect of the electron near an ALC. a) The electron spin relaxation (eSR) affects a reduction of the muon spin polarisation over time. b) Time-average of the muon spin polarisation curves. It can be seen that the eSR enhances the depth of the ALC signal.

In a further step, the electron spin relaxation can be included. This is achieved by adding the electron and mixed polarisation $\vec{P}_{\mathrm{e}} = (p_{\mathrm{e}}^{\mathrm{x}}, p_{\mathrm{e}}^{\mathrm{y}}, p_{\mathrm{e}}^{\mathrm{z}})^{\mathrm{T}}$ and $p_{\mathrm{mix}}^{\mathrm{jk}}$ to the spin density matrix:

$$\rho(t) = \frac{1}{4}\left(1 + \vec{P}_\mu(t)\cdot\vec{\sigma} + \vec{P}_{\mathrm{e}}(t)\cdot\vec{\tau} + \sum_{\mathrm{j,k}} p_{\mathrm{mix}}^{\mathrm{jk}}\sigma^{\mathrm{j}}\tau^{\mathrm{k}}\right), \tag{49}$$

where j and k correspond to x, y, and z indicating the components of the Pauli matrices $\vec{\tau}$ and $\vec{\sigma}$ of the electron and muon. The quantum mechanical equation of motion provides a set of 15 or, if a nuclear spin is included, 63 coupled differential equations [54, 55]. Assuming that the electron spins relax at a rate of λ_{eSR}, the set of

differential equations has to be expanded to [54]

$$\frac{\mathrm{d}p_{\mathrm{e}}^{\mathrm{j}}}{\mathrm{d}t} = \epsilon_{\mathrm{jkl}}\left[\frac{\omega_0}{2}p^{\mathrm{kl}} + \frac{\omega^*}{2}p^{\mathrm{ml}}n_{\mathrm{k}}n_{\mathrm{m}} + \omega_{\mathrm{e}}^{\mathrm{k}}p_{\mathrm{e}}^{\mathrm{l}}\right] - \lambda_{\mathrm{eSR}}p_{\mathrm{e}}^{\mathrm{j}}, \tag{50}$$

$$\frac{\mathrm{d}p^{\mathrm{jk}}}{\mathrm{d}t} = \epsilon_{\mathrm{nlm}}\left[\delta_{\mathrm{j,m}}\delta_{\mathrm{k,n}}\frac{\omega_0}{2}\left(p_{\mu}^{\mathrm{l}} - p_{\mathrm{e}}^{\mathrm{l}}\right) - \delta_{\mathrm{j,n}}\left[\frac{\omega^*}{2}n_{\mathrm{m}}n_{\mathrm{k}}p_{\mu}^{\mathrm{l}} - \omega_{\mu}^{\mathrm{m}}p^{\mathrm{lk}}\right]\right.$$
$$\left.+\delta_{\mathrm{k,n}}\left[\frac{\omega^*}{2}n_{\mathrm{j}}n_{\mathrm{l}}p_{\mathrm{e}}^{\mathrm{m}} - \omega_{\mathrm{e}}^{\mathrm{l}}p^{\mathrm{jm}}\right]\right] - \lambda_{\mathrm{eSR}}p^{\mathrm{jk}}, \tag{51}$$

which are defined by the commutators $\left[\sigma^{\mathrm{j}}, \sigma^{\mathrm{k}}\right] = 2i\epsilon_{\mathrm{jkl}}\sigma^{\mathrm{l}}$ and $\left[\sigma^{\mathrm{j}}\tau^{\mathrm{m}}, \sigma^{\mathrm{k}}\tau^{\mathrm{n}}\right] = 2i\left(\delta_{\mathrm{j,k}}\epsilon_{\mathrm{mnr}}\sigma^{\mathrm{r}} + \delta_{\mathrm{m,n}}\epsilon_{\mathrm{jkl}}\sigma^{\mathrm{l}}\right)$, the normal vector along the symmetry axis (axial symmetry) $\vec{n}$ and the hyperfine interaction parameters ω_0 and ω^* that depend on the host material. The indices correspond again to the coordinates x, y and z. This set of equations can generally not be solved analytically, but requires numerical simulations. The electron spin relaxation (eSR) gives rise to a relaxation of the muon spin polarisation that is superimposed on the damped Rabi oscillations as shown in Figure 10a. It is evident that this additional relaxation over time also reduces the time-averaged muon spin polarisation. In that sense, the electron spin relaxation leads to an increase of the magnitude of the ALC feature as shown in Figure 10b. Although the amplitude of the ALC increases, there are hardly any implications on the position and the width of the ALC when the electron spin relaxation rate is less than about 1 MHz. Fortunately, where this technique to access the electron spin relaxation rate is most applicable (in organic semiconductors), the values are typically lower than 1 MHz [52, 47].

2.4. Muon polarisation functions for muoniated radical states

As discussed above, in the limit of small or zero dynamics, there is very little or no relaxation of the muon's spin. Many experiments (discussed later in this review) have been conducted on organic materials, where relaxation rates have been analysed to extract electron spin dynamics. For example, muons have been extensively used to probe the properties of mobile spin excitations in various polymers. In these studies, the main source of muon relaxation has been attributed to HF coupling between muons bonded to the polymer and mobile electronic excitations, which are able to move relatively freely along the polymer chain. The motion of this electron, which can also be termed as a polaron, causes a time-dependent fluctuation of the HF interaction and consequently a reduction of the muon spin polarisation. Initially, the data were analysed using an exponential relaxation function and the expression used to extract diffusion rates from the relaxation rate was originally derived for NMR in an anisotropic system with diffusive spin motion. The exponential relaxation rate is given by [56, 57]

$$\lambda = \frac{\rho}{20}\left[3D^2 f(\omega_\mu) + 5A^2 + 7D^2)f(\omega_e)\right] \tag{52}$$

where ρ is the spin concentration and $f(\omega)$ is the spectral density function containing information on the spin dynamics, and the remaining symbols have been previously defined.

For a purely one-dimensional (1D) diffusion process, the correlation function for a particle revisiting the origin has a $t^{1/2}$ behaviour, so the associated spectral density derived by Fourier transformation is $f(\omega) \propto \omega^{1/2}$. This implies that the relaxation rate should follow a $B^{1/2}$ scaling law. Interchain motion is expected to provide a cut-off to the measured relaxation rate and can be included in the conventional relaxation rate theory by generalizing the motion to an anisotropic random walk on a discrete lattice and is given by [58, 59]

$$f(\omega) = \frac{1}{\sqrt{4\mathcal{D}_{||}\mathcal{D}_{\perp}}}\sqrt{\frac{1+\sqrt{1+(\omega/2\mathcal{D}_{\perp})^2}}{1+(\omega/2\mathcal{D}_{\perp})^2}} \tag{53}$$

in the limit of $\omega << \mathcal{D}_{||}$, where $\mathcal{D}_{||}$ is the on-chain diffusion rate and $\mathcal{D}_{\perp}$ the off-chain diffusion rate.

However, it is known that the correlation function for 1D diffusion is not an exponential and hence the muon spin relaxation is not expected to be a simple exponential either. Furthermore, since the correlation time for the return to the origin of a particle diffusing in 1D is divergent, the standard NMR theory is not strictly valid, as it assumes the existence of a finite correlation time that is short compared to all other timescales in the problem.

A more appropriate model is the stochastic diffusion theory to the model of a static muon interacting through an intermittent HF coupling with an electron that is randomly diffusing along a 1D chain. Risch and Kehr derived the corresponding non-exponential relaxation function and obtained an inverse field dependence for the relaxation parameter [60]. In general, the relaxation of the muon spin in a LF measurement on conductive polymers and many other organic systems is well described by the Risch-Kehr (RK) theory, which results in a relaxation function of the form

$$G(t) = \exp(\Gamma t)\mathrm{erfc}(\sqrt[2]{\Gamma t}) \tag{54}$$

where erfc is a complementary error function and the relaxation parameter is Γ, which is found to be inversely proportional to the square of the diffusion rate along the chain. If the polaron motion is mainly one dimensional, an inverse dependence of Γ on the applied magnetic field is expected. However, being a 1D stochastic theory, the Risch Kehr model is not able to handle systems with higher dimensional transport, and there is no explicit way of taking account of polaron loss via intra-chain hopping or trapped states brought about by impurities or structural defects. This latter point can be somewhat rectified by adapting Equation 53.

However, more generally, all of the ways of quantitatively extracting charge carrier hopping frequencies from the muon spin relaxation have an underlying problem. Since the muon spin relaxation function is a superposition of all muonium states in the system (whether the electron is localised to the muon or hopping between different sites), one must have a complete understanding of all of them in order to extract hopping rates. This includes the full muon-electron hyperfine tensor of all states, the proton-electron hyperfine tensor for all protons that are relevant for each muonium state, as well as other dynamics present in the system (such as a fluctuation of the hyperfine parameters and/or electron spin relaxation). It is not always possible to gain this information, especially for the delocalised states and when it is, a large number of different experimental measurements are required, coupled with a considerable amount of modelling. If the underlying muon spin relaxation in organic materials is dominated by another mechanism, electron spin relaxation for example, then the time dependence

of the relaxation will mimic the functional form this driving mechanism. For the case of electron spin relaxation, this is often an exponential. Indeed, the origin of this off-resonant muon spin relaxation in organic semiconductors is currently unresolved, and we discuss some of the issues in detail in Section 5.

As a concluding remark, we note that Section 2.3 and 2.4 merely outline many of the underlying principles and mathematics of muonium as a probe of materials, with an emphasis on the background of those topics that are currently research active. For further details, we direct the interested reader to one of the other reviews, books or original manuscripts [4, 8, 48, 61].

2.5. Advanced μSR techniques

2.5.1. Low energy muons Until around a decade ago, one of the main restrictions of the muon technique was its limitation to bulk investigations, since the surface muon's energy of 4.2 MeV results in a stopping distance in most materials of hundreds of microns. Thin films, multilayers and near-surface regions of materials could not be probed, which clearly are of increasing importance in contemporary condensed-matter science. For example, many thin films and heterostructures possess fascinating properties due to the reduced dimensionality; as a consequence of breaking the translational symmetry at a surface or interface, one expects a different behaviour from bulk materials. Moreover, close contact of materials with different order parameters leads to complex coexistence and competition phenomena, proximity effects, or new electronic states.

To be useful for thin-film and surface investigations, polarised beams with energies in the range of keV are needed, which result in the implantation depths into materials on the nm lengthscale. Several methods have been proposed to produce low energy muons. The primary concerns when proposing solutions is that the muons must retain their spin polarisation, the energy must be tuneable, the muons must have as small an energy uncertainty as possible and the conversion from high to low energy muons must be efficient enough to allow viable experiments. The main methods that have been actively pursued are the moderation muons in cryosolid films at PSI [62, 63, 64, 65, 66] and the laser ionization of thermal muonium at KEK, and later at RIKEN-RAL [67, 69]. The RIKEN-RAL beamline produces a pulsed low-energy muon beam with a muon energy tuneable between 1 and 10 keV, a time spread of around 8 ns, an intensity of around 20 muons per second with a spin polarisation of 50%. This technique's full potential will be developed at J-PARC, where a higher-flux beam line is currently being developed. In a particular exciting development, there are plans to build a muon magnetic microscope with a spot size of around 1 μm [68]. The method developed at PSI provides a quasi-continuous beam of 100% polarised muons, with an energy tuneable between 0.5 and 30 keV, a time spread of around 5 ns and an intensity of around 1000 muons per second. A dedicated experimental setup is routinely being used for depth-dependent measurements on a nm scale, as part of the external user programme. As a result, since the dedicated spectrometer was commissioned in 2006, more than forty articles have been published using the technique, which include papers on superconductivity [70, 71, 72], magnetism [73, 74], spin glasses [75], semiconductors [73, 76] and spintronics [78, 79].

Further details on the technique, and its applications, can be found elsewhere [62, 63, 64, 65, 66, 67, 69] and some specific examples of its application are discussed below.

2.5.2. Radio-frequency μSR Radio Frequency μSR, usually abbreviated to RF-μSR, is a technique similar to ESR or NMR. It is an extension of the μSR method that involves application of one or more radio frequency pulses to a sample, to stimulate either the implanted muons, or the sample nuclei, or both. This technique was pioneered by the ISIS facility, which is best suited to the application of pulsed RF signals as the RF pulsed can be timed with respect to the muon pulse. The timing of the RF pulse can be changed with respect to the muon pulse, such that the state-changes brought about by the RF pulse can be tracked as a function of time. Moreover, multi-pulse techniques similar to those used in NMR are possible. RF-μSR can be used, for example, to increase the frequency limit of ISIS, from around 10 MHz up to many hundreds of MHz. It is also possible to decouple the nuclear spins from the muon's spin, simplifying analysis of complex spin systems. Further details of the technique can be found elsewhere [80].

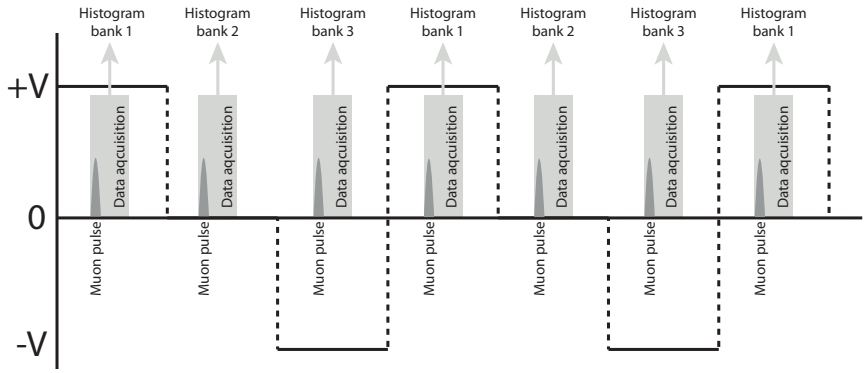

Figure 11: The timing structure of the electric field, muon pulse and data acquisition. In this figure, the separation of the muon pulses is dramatically reduced - in a real experiment, data acquisition is only about 30 μs, whereas muon pulse separation is 20 ms. The data is saved in a different set (bank) of histograms for each voltage setting. The voltage is continuously cycled between the different polairities and zero. This setup allows systematic changes to the sample or beam position to be averaged out.

2.5.3. Electric fields It is also possible to apply an electric field to a sample [81, 82]. At continuous sources, this will typically be a DC electric field. At pulsed sources, it is possible to modify the electric field between the pulses, allowing one to concurrently measure two polarities of the electric field as well as zero, with the data gated to different histograms, as shown in Figure 11. It is useful to investigate how, for example, how electrons drift by the muon in a semiconductor, or to study magnetoelectric coupling in multiferroic materials.

2.5.4. Laser excitation Another tool in the arsenal is light. Initially, researchers used flash lamps to perform photo-μSR experiments. Even today the flash lamp is an easy method to photo-excite samples [83], because the laser system tends to be expensive, takes up a lot of space, and requires high safety protocol. However, drawbacks are of course the low power density, long pulse duration (tens of μs), and broad spectrum. Historically, pulsed muon sources have been utilised to conduct

photo-μSR experiments because it can be easily coupled to the laser system for pulsed stimulation by synching the pulse timings. By changing the trigger timings, the laser pulse can illuminate on the sample before or after the muon pulse, which enables one to observe the dynamics at an arbitrary timing (unrelated to the intrinsic temporal window of the muon). This also has the advantage of being able to measure time-scales of excited states without having to know the underlying physics of how the muons couple to the excitation (needed to interpret the relaxation rates directly) [85]. This is schematically shown in Figure 12.

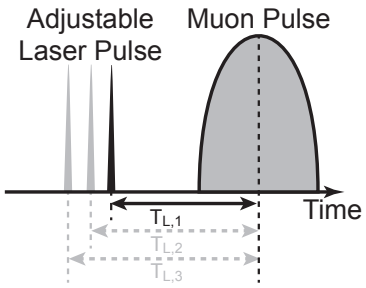

Figure 12: The pump-probe pulse structure. The pump (laser) timing can be changed relative to the probe (muons) to extract time dependency of the excitations. T_L can be varied to allow the laser to arrive before or during the muon pulse, as well as during the acquisition time but after the muon pulse.

The RIKEN-RAL Port-2 at the ISIS facility in the UK is currently the only muon beam line used for materials research with a laser setup. The laser system is based on a Continuum Panther EX OPO, pumped by a Nd:YAG Continuum Powerlite 9025 laser. The OPO takes 355 nm for pump laser and the OPO signal and idler can be frequency doubled to generate the second harmonic wavelength in the UV range. Therefore the output wavelengths cover almost the whole spectrum ranging from 210 nm to 2200 nm except the degeneracy wavelength at 710 nm. Although the output energy depends on the wavelength, the peak pulse energies are 50 mJ/pulse at 405 nm for the signal, and 20 mJ/pulse at 840 nm for the idler. The near-field beam profile is top-hat with an elliptical shape, however, since the laser beam propagates down a long light-tight beam duct connecting the laser cabin and the spectrometer, the beam profile is deformed by the time when it reaches the sample because of the multi-transverse mode structure. Fleming et al. utilised an evacuated image relay tube to transport the Nd-YAG 2nd harmonic (532 nm) beam to maintain the beam quality [84]. Recently, work has begun to upgrade the HiFi spectrometer at ISIS with a similar but higher power laser, to allow photo-excited states to be studied with muons at high magnetic fields (up to 5T) [85, 86]. Specifically, it will be used to access the wealth of science about electron dynamics in soft-matter systems, where one needs to tune to ALC resonances which typically occur at magnetic fields greater than 1 T in organic materials. Further information on the new setup, and some potential applications, can be found elsewhere [85].

3. μSR used to study inorganic magnetic systems

The μSR technique has several unique advantages when used to study magnetic systems. Due to the relatively large magnetic moment of the muon, the technique is sensitive to extremely small internal fields. The local probe nature of the muon makes it very sensitive to spatially and/or temporally inhomogeneous magnetism, so it is an ideal probe of critical behaviour above magnetic transition temperatures, or highly disordered or frustrated systems. Moreover, the occurrence of different phases in the sample will be reflected by different components in the signal and a careful analysis of the amplitude of these components furnishes a direct measure of the fraction of the sample involved in a particular phase. The technique can therefore be used to check the coexistence of different types of ground states at the microscopic level, as it is possible to independently extract the value of any static moment, any spin dynamics present and the sample volume involved in the various magnetic phases, which may not be picked up directly by other techniques. Similarly, μSR is a powerful tool when the magnetic order is short-ranged or disorder is too high for these other techniques.

3.1. Critical point spin dynamics

When a system is at or close to a critical point - for example, close to the Curie temperature of a ferromagnet - anomalies can exist in a wide variety of static and dynamic properties of the system. When studying a magnetic material close to a critical point with muons, one is mainly interested in the temperature dependence of the spontaneous field at the muon site (which probes the static magnetism) and in the spin lattice relaxation rate (probing the dynamics). A particular advantage of the muon technique, compared to for example NMR, is that it can be performed in zero magnetic field. This avoids any possible influence of the applied magnetic field on the spin dynamics, which is dreadfully important when studying magnetic systems, particularly those with weak interactions or moments.

The first detailed study of critical fluctuations was not carried out at one of the dedicated facilities we currently enjoy, but instead at CERN in 1984 [87], where it was technically challenging to perform zero and longitudinal field studies. Critical exponents were extracted from the relaxation rate data taken in the antiferromagnet MnF_2. The measurements were repeated at TRIUMF, which operates dedicated beamlines and sample environments for materials research, where the presence of strong anisotropy in the spin dynamics was confirmed [88].

Critical dynamics were investigated in the metallic ferromagnets Ni and Fe [89, 90], where it was shown that the dipolar interaction between the lattice dipole magnetic moments has a strong influence on the paramagnetic critical dynamics for small wave-vector modes [91]. This dipole interaction does not affect the ferromagnetic critical temperature T_c, and other methods proved challenging to study the critical dynamics which were of importance to understanding these transition metal magnets [90].

The manganites have also been studied [19, 92]. Evidence for a broad distribution of very slow and spatially inhomogenous Mn-ion spin-spin correlation times near and below the critical temperature was presented in (La,Ca)MnO_3 [92]. These spin correlations are not observed in traditional ferromagnets, where spin excitations tend to dominate. The authors suggest that the inhomogeneous spin dynamics may be from a glassy state, and that since the nature of the technique is a real-space local probe, it

could be that the ground state of these complex materials is not homogeneous. It was believed that at optimal doping of this system, the magnetism is homogeneous. But muons showed that there are multiple relaxation channels below T_c [43, 93, 94, 95], which have been interpreted as conducting regions forming as the temperature is lowered below T_c. For a detailed discussion of the series of results reported, and a discussion of their context, we direct the readers to a review written by some of the key researchers in this field [19].

One of the systems that has been extensively studied is the intermetallic ferromagnets. For example, $GdNi_5$ is an axial ferromagnet with a critical temperature of approximately T_c ~31 K [96]. It is characterised by extremely weak magnetic anisotropy arising from the dipole moment interaction between the Gd^{3+}. ZF muon measurements were performed as a function of temperature on two crystalline samples with different orientations with respect to the muon's initial spin direction (c-axis either parallel or perpendicular to the muon's spin) [96]. It was shown that above T_c, the relaxation rate is temperature independent, reflecting the vanishing pair correlations at high temperature, as a result of the relatively low density of states at the Fermi level [97]. Below T_c, the muon spin relaxation is driven by spin waves - a two magnon process, such that the relaxation rate follows a $T^2 \ln T$ law. From fits to the data, a magnon stiffness constant is reported.

Perhaps one of the most important discoveries in the $GdNi_5$ system is in relation to testing the hypothesis of dynamical scaling, an extension to static scaling theory of phase transitions. The relaxation rate measured close to T_c is a weighted sum of two functions, to express longitudinal and transverse fluctuations. The longitudinal fluctuations saturate as T_c is approached, whereas the transverse ones diverge [96]. It was shown that the critical dynamics above and below T_c are very similar to one another, which supports the scaling theory of critical dynamics [98].

Since these early studies on critical dynamics, there has been interest more recently in studying quantum critical dynamics, close to a quantum critical point (QCP). Temperatures as low as 20 mK can be routinely achieved on a muon beamline, and the dynamic sensitivity and localised nature of the probe make it an ideal technique for studying this physics. For example, muon experiments were carried out on $YbRh_2Si_2$, a compound that exhibits non-Fermi-liquid (NFL) behaviour associated with a QCP [99]. The zero-field muon relaxation rate was found to be independent of temperature down to 100 mK, but increases at around 70 mK, which is consistent with a QCP. The relaxation was found to obey a time-field scaling relation that suggests long-lived spin correlations at low temperatures. Muon spin relaxation measurements on $CeInPt_4$ reveal that below 1 K, the electronic relaxation rate increases without any loss of muon initial asymmetry, indicating the presence of low energy spin fluctuations. When combined with heat capacity data, it is suggested that $CeInPt_4$ may exhibit NFL behaviour close to a QCP [100]. Low-energy spin dynamics have also been investigated near the ferromagnetic QCP critical point in $CePd_{0.15}Rh_{0.85}$, where again a slowing down of the spin fluctuations with decreasing temperatures below 2 K is observed (consistent with a QCP) but there is no clear sign of either static long-range magnetic ordering or spin freezing down to 60 mK [101]. In addition to showing that QCPs exist, muons are also a useful tool for verifying if other spin dynamics are present. CeFePO was studied by muon-spin relaxation and short-range static magnetism was shown to occur at around 0.7 K, which prevents the emergence of a ferromagnetic QCP in this system [102]. Finally, the non-centrosymmetric heavy fermion antiferromagnet $CeRhSi_3$ has been investigated with muons, where a monotonic suppression of the

internal fields was observed upon an increase of external pressure. The data suggest that the ordered moments are quenched with increasing pressure. At 23.6 kbar, the ordered magnetic moments are fully suppressed, suggesting that they directly observed the quantum critical point hidden inside the superconducting phase [103].

3.2. Spin glasses, liquids and ices

Frustration arises in magnetic systems from competing exchange interactions and if this frustration is randomly distributed whilst being present at a sufficient density, then long-ranged magnetic order is not possible. In some materials, the level of frustration is a tuneable quantity, so in principle the evolution in behaviour can be studied as the material changes from all ferromagnetic to all antiferromagnetic. Introducing AF bonds leads to a reduction of the ferromagnetic critical (ordering) temperature and beyond a critical concentration of frustration, there is a loss of long-ranged order and the development of a spin glass.

The first spin glasses that were recognised as such were dilute metallic alloys of a magnetic transition metal element (such as Fe) in a non-magnetic host (such as Cu). Since their initial discovery [104, 105], it was realised that spin glasses were of great interest as magnetic examples of the much more general class of glassy materials. It was soon discovered that the spin glass label could be applied to many examples outside the original dilute alloys, and since then hundreds of systems have been discovered in a wide variety of materials. One of the phenomena that has been most extensively investigated is the slow relaxation dynamics that occurs below the glass transition temperature T_g [+]. Another phenomenon that has been investigated is the anomalous non-exponential spin relaxation above T_g.

Muons are ideal to study both of these phenomena, as they are able to probe slowly relaxing systems with a wide relaxation rate spectrum. Pioneering measurements on CuMn first showed qualitatively that there was a rapid increase of muon relaxation rate at T_g [106]. The temperature dependence of the spin glass relaxation time was estimated for the first time in AgMn [107, 108] and extensive analysis of AuFe and CuMn alloys was performed in terms of the coexisting static and dynamic random fields [109], addressing in particular the differing muon sites in the dilute magnetic alloys. These three sets of experiments put limits on the models used to describe the freezing process. They showed that freezing is not a process where some spins become static, gradually joined by others as the temperature is lowered. Instead, it was shown that spin glass freezing is a cooperative effect where all spins develop a static component as they are cooled below T_g.

As well as standard spin glasses, reentrant systems where spin glasses appear below the Curie temperature of ferromagnets have been studied. For instance, AuFe is a spin glass at one end of the concentration range and ferromagnetic at the other, but within the ferromagnetic region ordering is complex [110, 111]. As the temperature is decreased for a fixed concentration beyond the critical concentration needed for ferromagnetism, there is an onset of ferromagnetism and at lower temperatures there is a spin canting, where the spin components perpendicular to the magnetisation direction freeze without loss of ferromagnetic order parallel to the domain magnetisation. At lower temperatures still, low energy fluctuations appear; there is an increase in the muon spin relaxation rate [112, 113] which is related to slow fluctuations corresponding to the spin glass.

[+] commonly referred to as a "freezing temperature" in the literature.

Experiments on spin glasses above T_g with a moderate concentration show muon spin relaxation that appears to be of stretched exponential form, with the stretch parameter varying from 1 at high temperatures (corresponding to an exponential function) to 1/3 as T_g is approached [114]. This behaviour is rather general, with many different systems following the same behaviour, including canonical, metallic, insulating, semiconducting and pyrochlore spin glasses[114, 115, 116, 117, 118, 119]. After careful consideration of geometrical and muon stopping site issues, involving the nature of dipolar moment coupling with muons in dilute spin systems, it was clear that this temperature dependent stretched exponential form of relaxation is related to a wide spectrum of local spin fluctuation rates combined with non-exponential relaxation at individual muon sites [120, 121]. Perhaps the most useful way of quantitatively analysing the muon data in spin glasses, however, is to invert the muon relaxation function into a local spin autocorrelation function of the material [114, 122, 123]. The result is an apparent universal dynamic behaviour in spin glasses, which itself can be generalised to the dynamics in all glasses. However, the exact nature of the spin glass ground state and the low lying excitations are still an unsettled theoretical problem [75].

More recently, the complex magnetism in materials which were originally considered to be spin glass candidates has been investigated with muons. For example, $LiHo_xY_{1-x}F_4$ is ferromagnetic for $0.25 \leqslant x \leqslant 1$ and it was believed that for $x < 0.25$, in this most diluted regime, the long ranged dipolar interactions with the chemical disorder produced a spin glass ground state. The ac susceptibility data for $0.1 \leqslant x \leqslant 0.25$ were interpreted by the authors as a transition to a low temperature spin glass state, which was supported by numerical calculations [124, 125, 126, 127]. In contrast recent muon measurements did not find canonical spin glass behaviour down to 15 mK. Instead, below 300 mK temperature-independent dynamic magnetism was observed that was characterised by a single correlation time. Importantly, the 300 mK energy scale corresponds to the Ho^{3+} hyperfine interaction strength, suggesting it may be involved in the dynamic behaviour of the system [128]. Another system where spin glass behaviour has been ruled out with muon measurements is the pyrochlore $Eu_2Ir_2O_7$. Early studies indicated spin-glass-like behaviour on the basis of bifurcation of field-cooled (FC) and zero-field-cooled (ZFC) magnetisations and little or no specific heat anomaly at a transition temperature [129]. However, muon measurements revealed a uniform spontaneous local field indicating long-range magnetic order, ruling out both quantum-spin-liquid (within the muon time window) and spin-glass-like ground states [130]. It is worth noting that the precise meaning of "long-range order" in magnetic materials is a matter of some complexity. Indeed, it has recently been shown that over damped precession can be observed in materials with only short-range quasi-static correlations [131]. In the case of the long-range order reported for $Eu_2Ir_2O_7$ [130], a significant number of oscillations are observed in the muon spectra (i.e it isn't over damped) and so the correlation length significantly exceeds 10 unit cells. Further information on this rather complex point of correlation lengths can be found elsewhere [8, 131].

Indeed, pyrochlore systems have been extensively studied by muons. A quick literature search involving the terms 'pyrochore' and 'muon' reveals around 80 publications, dating back to the 1990's (see, for example, ref [132]). The combination of a negative exchange constant (normally associated with antiferromagnetism) and certain triangular lattice symmetries results in phenomena known as geometrical frustration, and pyrochlores exhibit this in abundance. Systems studied include

$Tb_2Ti_2O_7$ and $Yb_2Ti_2O_7$ which are believed to be in a quantum fluctuation regime at low temperatures [132, 133] and are spin-liquid candidates (see the discussion below), $Gd_3Ga_5O_{12}$ where a linear decrease in the Gd spin fluctuation rate is observed as temperature is decreased [134], $Gd_2Ti_2O_7$ and $Tb_2Sn_2O_7$ where spin dynamics and magnetic order are shown to co-exist down to temperatures as low as 20 mK [135, 136, 137] and $Cd_2Re_2O_7$ where two distinctive types of localised states are found, with characteristic radii of about 0.5 and 0.15 nm. These states have been explained in terms of spin polarons [138].

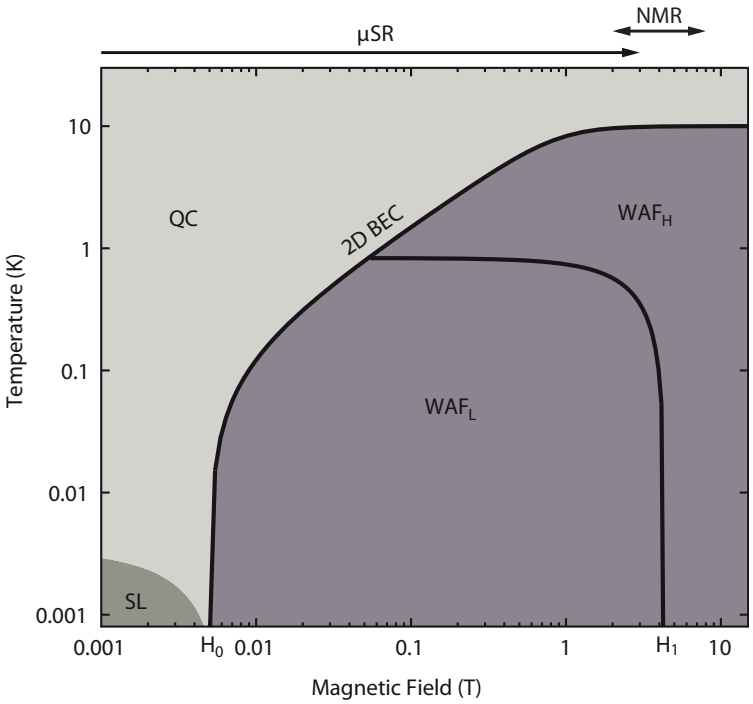

Figure 13: The finite-temperature H-T phase diagram for κ-(BEDT-TTF)$_2$Cu$_2$(CN)$_3$ obtained from muon, NMR and thermodynamic measurements. The respective field ranges for the muon and NMR techniques are indicated. The most important feature of the phase diagram is the presence of two quantum critical points at the magnetic field values H_0 and H_1. The quantum critical (QC) and weak-moment antiferromagnetic (WAF) regions are shown, with the WAF region subdivided on the basis of the behaviour of its characteristic critical parameters (L, low; H, high) [140]. SL is the gapped-spin-liquid regime. Adapted from the original figure [140].

In contrast to a spin glass, a quantum spin liquid is a disordered state which preserves its dynamical disorder to very low temperatures. In this state, all magnetic correlation functions are short ranged [139] and the magnetically ordered ground state is avoided due to strong quantum fluctuations [140]. Whilst it was first predicted theoretically in 1973 [141], it is only until very recently that materials have become available that exhibit persuasive experimental evidence for such a state [142]. The layered molecular system κ-(BEDT- TTF)$_2$Cu$_2$(CN)$_3$ is a prime example of a

spin liquid*, which despite having a high-temperature exchange coupling of 250 K, shows no obvious signature of conventional magnetic ordering down to 20 mK [140]. Recent muon measurements show that by applying a small magnetic field H_0, one is able to produce a quantum phase transition between the spin-liquid phase and an antiferromagnetic phase with a strongly suppressed moment [140]. Moreover, at a higher field H_1, a second quantum critical transition is observed which could be related to a threshold for deconfinement of the spin excitations. Shown in Figure 13 is the low temperature magnetic phase diagram of this spin liquid [140].

The insulating pyrochlore $Tb_2Ti_2O_7$ is also a three-dimensional spin liquid candidate. The strength of the exchange interaction should induce magnetic order at approximately 20 K, but according to muon-spin relaxation and neutron scattering measurements, it is still in a correlated paramagnetic state down to a temperature of 0.05 K [132, 143]. Yaouanc et al. have recently published a detailed experimental investigation showing that an exotic phase transition takes place at T = 0.15 K [144], characterised by an anomaly in the muon precession frequency which is not observed in the specific heat. The authors suggest that it might be associated with a cooperative Jahn-Teller transition. In a more recent paper, Yaouanc et al. discuss how the short-range spin correlations in spin liquids affect the muon spin relaxation spectra [131], and compare it to muon data taken on $Yb_2Ti_2O_7$. They find that the shape of the zero-field relaxation function is highly sensitive to short-range spin correlations, and that the field distribution at the muon site is found to be strongly asymmetric (it deviates substantially from the expected Gaussian function).

Another structure susceptible to exhibiting spin liquid behaviour is the Kagome lattice. Muon spin relaxation measurements have recently been reported on $Mg_xCu_{4-x}(OH)_6Cl_2$ with x close to 1. This material exhibits regular Kagome planes of S = 1/2 ions (Cu^{2+})[145]. A detailed investigation of the spin dynamics is presented and a defect-based interpretation is proposed to explain the unconventional dynamics observed in the quantum spin-liquid phase. The inter-site defects give rise to a distribution of couplings that can consistently explain the observed μSR and neutron results by employing the fluctuation dissipation theorem. The vanadium oxyfluoride $[NH_4]_2[C_7H_{14}N][V_7O_6F_{18}]$ (DQVOF) is a geometrically frustrated magnetic bilayer material, whose structure consists of S = 1/2 Kagome planes of V^{4+} d^1 ions with S = 1 V^{3+} d^2 ions located between the Kagome layers. Muon spin relaxation measurements demonstrate the absence of spin freezing down to 40 mK despite an energy scale of 60 K for antiferromagnetic exchange interactions. From combined muon, magnetisation and heat capacity measurements, Clark et. al conclude that the S = 1 spins of the inter-plane V^{3+} ions are weakly coupled to the Kagome layers, such that DQVOF can be viewed as an experimental model for S = 1/2 Kagome physics, and that it displays a gapless spin liquid ground state [146].

Finally, one of the more controversial applications of muons in recent years concerns the claimed observation of a species in a spin ice that shares properties with magnetic monopoles [147]. The motivation of this study was the proposal that magnetic charges can exist in certain materials, in the form of emergent excitations that manifest in a similar way to point charges, or magnetic monopoles [148]. Using transverse field μSR measurements of the 'spin ice' $Dy_2Ti_2O_7$, Bramwell et al. showed a temperature dependent spin relaxation rate, interpreting it in terms of magnetic

* Although one might argue that this discussion belongs in Section 4 about organic magnetic materials, it sits rather nicely in this part of the discussion with the other spin liquids

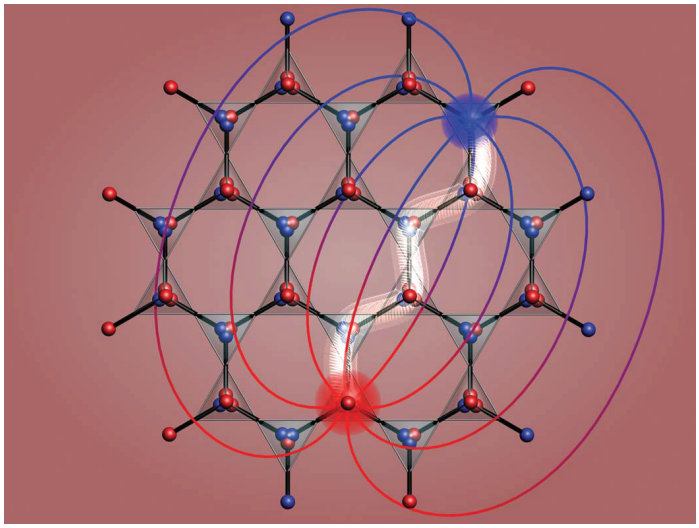

Figure 14: The ends of a chain of magnetic dipoles, highlighted in white, allegedly behave like magnetic monopole [147].

fluctuations resulting from magnetic monopoles, stating that it is consistent with the temperature and magnetic field dependence anticipated for monopole nucleation - the so-called second Wien effect [149]. These monopoles are illustrated in Figure 14. They put forward an elegant model, that involved no free parameters, to describe the temperature and magnetic field dependent monopole nucleation rate. They extract a value for the magnetic charge of $Q \sim 5\mu_B/\text{Å}$ [147], which is close to the value $Q \sim 4.6\mu_B/\text{Å}$ predicted by theory [148].

In addition to the lively debate in the conference circuit, specific criticism of the work by Bramwell et al. has recently been published [150, 151, 152].

In the first of such papers, Dunsiger et al. claim that the Bramwell et al. work is "flawed in its conceptual design and execution and incorrect in its theoretical interpretation of the muon spin depolarisation rate" [150]. Dunsiger et al. mounted their sample on a GaAs plate and performed a transverse field μSR, which is known to form 100% muonium and therefore results in no precession at the Larmor frequency. They show that at 100 mK, the signal from a pure GaAs plate and that of the $Dy_2Ti_2O_7$ mounted on a GaAs plate was identical beyond 1 μs. They conclude that there is no long-lived precession signal emanating from the specimen, and that the small difference observed at low times is a result of muons hitting the cryostat surroundings. Dunsiger et al. then go on to show that the ZF muon spin relaxation rate is temperature independent, contrasting the work of Bramwell et al., who showed a temperature dependent transverse field relaxation rate at low temperatures. A comparison of the two is shown in Figure 15. Dunsiger et al. noted that a stray field could be generated within the Ag plate used in the work by Bramwell et al. and that muons landing in such a region could undergo slow relaxation due to the inhomogeneous stray field. Indeed, these measurements and arguments appear to be

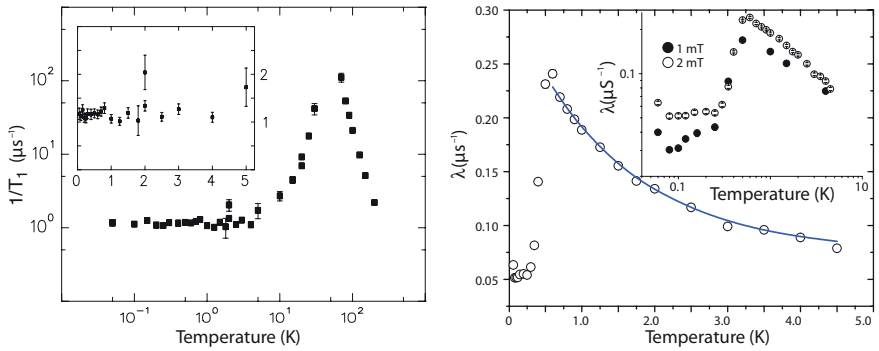

Figure 15: Comparison of the temperature dependence of the muon spin relaxation rates in $Dy_2Ti_2O_7$, by Dunsiger et al. and Bramwell et al. a) The muon spin relaxation rate analysed using a stretched exponential commonly used to model glassy systems. The low temperature behaviour is shown on an expanded linear scale in the inset, and is seen to be temperature independent. Figure adapted from Dunsiger et al. [150] b) Temperature dependence of the muon relaxation rate. The high temperature regime follows the expected activated behaviour. At low temperature, the relaxation rate depth is claimed to be proportional to the monopole concentration. Its rapid increase above 0.3 K marks a crossover from the regime of weak screening to strong screening of the charges. Inset, data on a logarithmic scale along with data taken in 1 mT. Figure adapted from Bramwell et al. [147].

quite convincing. However, the magnitude of the relaxation rates is relatively large in Dunsiger et al.'s measurements; presumably this is from a cryostat background, and it is likely to dominate the small relaxation rates observed by Bramwell et al. Moreover, the GaAs will likely result in the $Dy_2Ti_2O_7$ having a poor thermal contact with the cold-finger of the cryostat. It is not certain that the specimen was sufficiently cold to observe the monopoles reported in Bramwell et al.'s work. Finally, the measurements had relatively low counting statistics resulting in some potential difficulty when trying to observe small changes in slow relaxation rates.

The second paper is by S. Blundell, who argues a number of points [151]. Firstly, Blundell estimates that the monopoles are very sparse in a spin ice at very low temperatures, which means that only a small fraction of the implanted muons stop in the vicinity of a monopole. He then goes on to point out that the theory presented in Bramwell et al.'s work predicts that the experimentally measured quantity $m = \frac{1}{\lambda(0)}\frac{d\lambda(B)}{dB} \propto T^{-2}$, where $\lambda(B)$ is the relaxation rate at as a function of applied magnetic field, B, and T is temperature. Blundell replots Bramwell's data to show that $m \propto T^{-2}$ only holds for a very small subset of the data, and points out that given m is approximately constant below 0.3 K, a limited intersection with the hypothesised $m \propto T^{-2}$ curve is not unexpected even if the model is inapplicable. Blundell then goes on to argue, based on calculations and modelling, that the most likely explanation of the data presented by Bramwell et al. is that the observed relaxation rate originates from outside the sample (as implied by Dunsiger et al. [150]), as a direct result of static, macroscopic dipolar fields external to the sample.

Both Dunsiger et al. [150] and Blundell [151] note that the internal field at the muon site is likely too great to result in a TF precession signal, and this could indeed be an explanation of the effect that Bramwell et al. observed. Indeed, an earlier μSR study using longitudinal-field decoupling [153] showed that the field at the muon site was around 0.5 T, so that a 2 mT field (the maximum field used in Ref. [147]) would not be expected to lead to a precession signal.

In contrast, very recently in 2013, Chang et al. attempted to reproduce monopole result on a different spin ice system, $Ho_2Ti_2O_7$, using muons [154]. They draw a number of important conclusions from their work. Firstly, their results indicate that at higher temperatures, the dominant contribution to the muon relaxation rate arises from stray fields from the magnetised spin ice that penetrate into the silver sample plate, as suggested previously [150, 147]. However, a signal from muons implanted in the sample plate may not negate the important findings of the original study [155]. The second important conclusion of Chang et al.'s work is that their data are consistent with the original study of $Dy_2Ti_2O_7$ [147]. Chang et al. conclude that the Wien effect signal in $Ho_2Ti_2O_7$ arises from inside the sample or from within the Ag sample plate but at distances very close to the spin ice sample surface. Their experiments were very meticulous, and included: two separate experiments carried out three months apart (resulting in very similar data), a realignment of the $Ho_2Ti_2O_7$ disks between runs (resulting in very similar data), measurements on the more dilute $Ho_{2-x}Y_xTi_2O_7$ (the Wein effect appears to go away) and experiments with different thickness Ag foil (no large effect). All of these carefully carried out experiments combined demonstrate that the results cannot be attributed to instrumental effects, are reproducible under different conditions and the results are not particularly sensitive to the exact details of the sample geometry. Moreover, their use of Ho instead of Dy eliminates the possibility of material specific results. However, as has been recently pointed out, the $Dy_2Ti_2O_7$ results could also be interpreted as quantum diffusion of muons in the material [152]. In this scenario, the plateau observed at low temperature ($<$7 K) in the relaxation rate is due to coherent tunnelling of muons through a spatially disordered spin state and not to any magnetic fluctuations persisting at low temperature. It is conceivable that the $Ho_2Ti_2O_7$ results may also be interpreted in this way. However, muon measurements of $Y_2Ti_2O_7$ indicate there are temperature dependent low field fluctuations present[156], which have been interpreted as being down to muon diffusion. The hopping rate is found to be significantly slower than coherent diffusion in metals, which calls into question the argument that coherent diffusion is present at low temperatures in $Dy_2Ti_2O_7$.

It seems clear that there needs to be some further studies of various spin ice systems using different muon spectrometers and carried out by different groups, which will hopefully stimulate further debate and resolve the issues presented here.

3.3. Magnetic semiconductors

Dilute ferromagnetic semiconductors have been intensely studied because of their possible applications in spintronic devices. Thin films with high concentrations of magnetic ions are grown under conditions far from thermodynamic equilibrium, and show high sensitivity of their properties to preparation and heat treatment, demonstrated by a nearly 50% increase of the ordering temperature by annealing [157, 158]. Large peaks in the ac susceptibility observed well below the ferromagnetic transition temperature have been attributed to successive ferromagnetic transitions

of different regions [159]. Such inhomogeneities, if intrinsic, will have major negative impacts on device applications involving magnetisation manipulation and polarised spin injection.

Muon spin relaxation yields unique information about the volume fraction of regions having static magnetic order, as well as the size and distribution of the ordered moments [8, 10], so it is an ideal tool to study the supposed intrinsic inhomogeneous magnetism in dilute magnetic semiconductors [160]. A recent low-energy muon study by Storchak et al., reported that ferromagnetism develops in (Ga, Mn)As only in about half of the sample volume [161]. In contrast, using the same technique on similar samples, it has recently been reported by Dunsiger et al. that (Ga, Mn)As shows a sharp onset of ferromagnetic order, developing homogeneously in the full volume fraction, in both insulating and metallic films [73]. The contradictions between these two nominally identical measurements have been partly explained by an apparent subtle difference in preparation methods and/or growth conditions of the specimens. Dunsiger et al. also found significant inhomogeneity by μSR in a film prepared with different and less ideal MBE growth conditions. Moreover, they note that Storchak's results imply a magnetic moment of 2.0 Bohr magnetons per Mn, which is significantly smaller than the moment size obtained in their work.

Dunsiger et al. also note that Storchak et al. used the slowly relaxing asymmetry in zero-field to estimate the paramagnetic volume fraction, which generally includes a contribution from muons that stopped in sites where the static local fields from the ordered moments are parallel to the initial muon polarisation. This can lead to an overestimate of the paramagnetic volume fraction. Performing measurements in transverse fields can result in more reliable estimates of the non-magnetic volume fraction. Whatever the idiosyncracies of interpretation of these two studies, the important result is that the Dunsiger work suggests that magnetic inhomogeneities may not be intrinsic to this class of materials.

In addition to identifying magnetic volume fractions, understanding the underlying physics of some of the rather extreme phenomena in this class of materials is also needed. Transport properties of these materials exhibit quite remarkable temperature and magnetic field dependence. For example, the resistivity of doped EuSe [162], EuS [163] or EuO with O vacancies [164] changes by up to 13 orders of magnitude over a very small temperature range near the FM transition and magnetic fields of 10 T suppress these resistivity maxima by 3-4 orders of magnitude. The magnitude of these effects and their dependence on temperature and magnetic field can only be explained in terms of electron localization the size of a few unit cells; a magnetic polaron [165]. Although the consensus leaves little doubt about the existence of magnetic polarons, its direct observation is difficult.

Muon spin-rotation/relaxation measurements have been reported in the ferromagnetic semiconductor EuS [165]. High transverse field measurements in the paramagnetic state show frequency spectra that are attributed to a magnetic polaron, formed when the positive muon binds a free electron generated in the process of muon implantation. This is similar to that of muonium, which has been studied extensively in nonmagnetic semiconductors, but in the polaronic case, the binding of the electron is aided by the strong exchange interaction with the neighbouring rare-earth Eu^{2+} moments. This leads to the creation of a giant electronic spin around the muonium. It is argued that in the paramagnetic state, this giant spin is rapidly fluctuating and the muonium electron spin is strongly coupled to it. This would explain the two frequencies on either side of the free Larmor frequency in the paramagnetic regime, which then

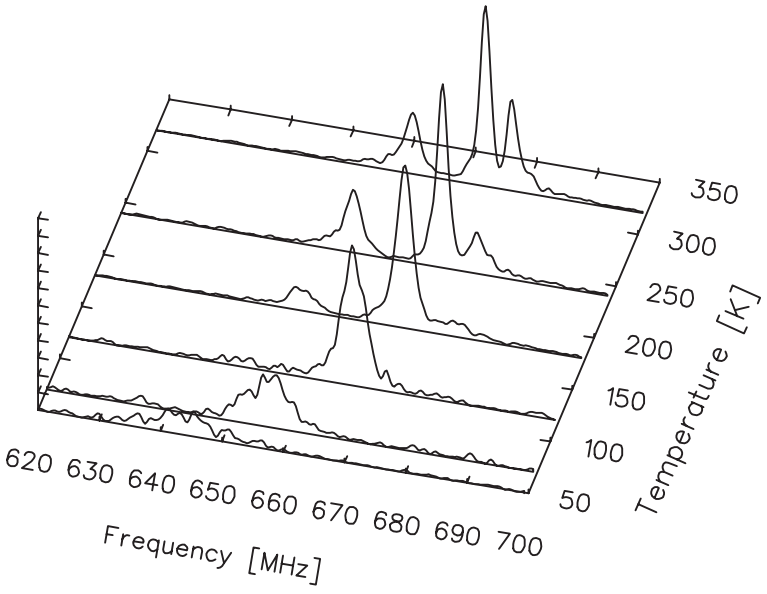

Figure 16: Fourier transforms of the muon-spin- precession signal in EuS in an external magnetic field of 5 T at different temperatures. As T decreases toward the Curie temperature 16.5 K, the bulk magnetisation increases, broadening and shifting all three lines; but the "satellite lines" attributed to the magnetic polaron are suppressed almost completely below 100 K [165].

disappear at low temperature since the bound magnetic polaron is destabilised by the ferromagnetic alignment of the neighbouring Eu^{2+} moments. The satellite peaks and their surpression below 100 K are shown in Figure 16. These features, it is argued, are a direct confirmation of the existence of a magnetic polaron.

However, it was subsequently pointed out that in the fast fluctuation limit, one expects the magnetic polaron spin and resulting hyperfine field on the muon to be rapidly fluctuating [166]. This leads to a single frequency, which is shifted relative to the Larmor frequency by an amount proportional to a Brillouin function associated with the large spin, but there is no evidence for any large attendant spin. It was suggested that the anomalous signal in EuS may be due to a small fraction of muons occupying the face-centre interstitial site which is occupied in isostructural compounds.

In reply, it was argued that there is an extremely strong interaction (on the order of tens of eV) of the f electrons within the Eu^{2+} ion (the primary reason for all seven electrons of the f shell forming spin 7/2) [167]. There is a strong (about 0.5 eV in EuS and EuO) $s - f$ exchange interaction of the magnetic polaron electron with nearest Eu ions. All other interactions are weaker, including crystal-field splittings, dipole interactions, or the hyperfine interaction between the muon and the magnetic polaron electron. Accordingly, this forbids any flip-flop transitions in the formation and dynamics of the magnetic polaron. Following further arguments in relation to the mechanism of a magnetic polaron in a ferromagnetic environment (as opposed to an antiferromagnetic one), it was argued that spin flip-flop interactions between

the magnetic polaron electron and an electron in the f shell of a neighbouring Eu^{2+} cannot average out a two-line hyperfine spectrum to yield a single line [167].

Finally, in a more recent work on EuO_{1-x}, it has been shown that static and homogeneous magnetic order persists up to an elevated critical temperature in the doped materials, and the results are incompatible with either the magnetic phase separation or bound magnetic polaron descriptions previously suggested, but are compatible with an RKKY-like interaction mediating magnetic interactions above 69 K [168].

3.4. Next generation energy materials

In recent years there has been a growing interest in characterising lithium insertion materials for Li-ion batteries. As a result, many potential battery materials have been characterised by muons (e.g $LiCoO_2$, $LiNiO_2$, and $LiCrO_2$), often with a focus on studying their magnetism. This is in part because there appears to be a correlation between the magnetic and/or electronic properties of the material and Li^+ diffusion, which is of course the basic principle behind the operation of Li-ion batteries.

The first demonstration that muons are able to measure Li^+ diffusion in battery electrodes was on $Li[Mn_{1.96}Li_{0.04}]O_4$, where a temperature dependent change of the field distribution width was attributed to the presence of Li^+ diffusion [169]. However, it was not possible to extract quantitative information about the Li^+ diffusion rate. A more recent example is the weak transverse field measurements performed on $LiCrO_2$. In this material, the Cr^{3+} ions form a two-dimensional triangular lattice in the CrO_2 plane. The muon measurements indicate the existence of a bulk antiferromagnetic phase at $T_N = 61.2$ K. Below T_N, ZF muon measurements demonstrated the formation of static long-range order, in agreement with neutron measurements, and no short-range order was shown to exist above T_N. A possible change from a low-temperature static state to a high-temperature dynamic state was found at 115 K, which was linked to potential motion of the Li^+ ions [170] despite it being electrochemically inactive. Unfortunately, later studies showed that Li^+ diffusion in $LiCrO_2$ does not become appreciable until at least 475 K [171].

Not long after this article on $LiCrO_2$ was published, a definitive paper was published that reported a direct measurement of the diffusion coefficient of Li^+ ions, D_{Li}, in Li_xCoO_2 [172]. Indeed, it was demonstrated that muons have some significant advantages over other techniques used to measure D_{Li}, in particular Li NMR. Although Li NMR is a powerful technique to measure D_{Li} for nonmagnetic materials, it is particularly difficult to quantitatively extract D_{Li} for materials containing magnetic ions, because the magnetic ions affect the spin-lattice relaxation rate from which D_{Li} can be estimated. Since Li insertion materials normally include transition metal ions, in order to maintain charge neutrality during the extraction and/or insertion of Li^+ ions, it is rather difficult to use NMR to estimate D_{Li}. This limitation is not present with the muon technique, as muons are not sensitive to the paramagnetic state at high temperature, but are sensitive to the change in nuclear dipole field due to Li diffusion. Shown in Figure 17 is D_{Li} estimated from muons for two concentrations of Li, which are in good agreement with theoretical calculations. It can also be seen that D_{Li} determined from Li NMR experiments underestimates the theoretical value, and is considerably lower than the value extracted from muon measurements, despite the elevated temperature at which the NMR measurements were taken.

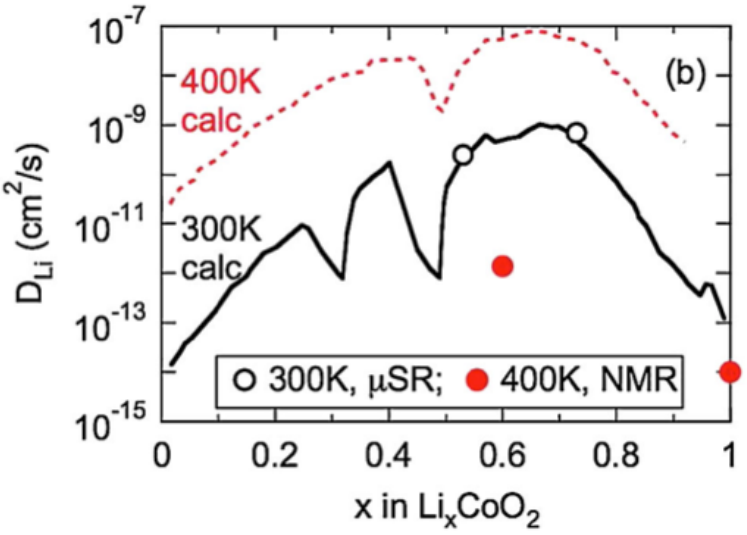

Figure 17: The relationship between D_{Li} and x in Li_xCoO_2 extracted from muon experiments (open circles). The solid line and the dashed line represent the predictions by first-principles calculations. The Li NMR result is also plotted (solid dot) for comparison, where it can be seen there is a considerable underestimate of D_{Li}.

Besides the interesting change in the magnetism of magnetic lithium ion insertion materials, magnetic ions are expected to reduce D_{Li} if doped into the Li layers, and the system $Li_{1-x}Ni_{1+x}O_2$ was explicitly chosen to investigate this phenomenon [171]. Prior to investigating D_{Li}, the magnetic ground state of Li_yNiO_2 ($0.1 \leqslant x \leqslant 1$) was investigated [173]. Until recently, there was no consistent picture about the nature of the magnetic ground state. Muon measurements suggest that static magnetic order incommensurate to the spatial lattice period for $y \geqslant 0.6$ is present at low temperatures, but neutron scattering measurements may be more appropriate to conclusively determine whether or not the magnetism is incommensurate [8, 174]. Disordered static magnetism due to localised Ni moments was confirmed for $1/2 \leqslant y \leqslant 1/4$ and $Li_{0.1}NiO_2$ was found to be non-magnetic [173]. The ground state of $LiNiO_2$ was inferred to be a static but short-ranged A-type AFM order [173]. The high temperature Li^+ diffusion was then investigated in $Li_{1-x}Ni_{1+x}O_2$ with x=0.02, 0.03, and 0.15, to elucidate the effect of Ni ions in the Li layer have on magnetism and Li^+ diffusion [171]. It was found that D_{Li} reduces strongly as one increases the amount of magnetic ion in the Li transport layer. By combining the results of experiments on Li^+ diffusion in $LiCrO_2$, $LiCoO_2$ and $LiNiO_2$, Sugiyama et al. were able to draw the conclusion that the temperature at which Li^+ begins to set in correlates with the material's electron-transport properties. That is, the material with an onset temperature of 150 K, Li_xCoO_2, shows metallic behaviour, the next lowest at close to 300 K is $LiNiO_2$ which shows semiconducting behaviour and $LiCrO_2$, with the highest onset temperature in excess of 475 K, is an insulator [172, 171]. However, more recent work on the insulating $LiFePO_4$ shows that the Li^+ diffusion is very large, too large in fact for muons to measure at 260 K, with an onset closer to 150 K [175]. There is yet, however, no direct link found between magnetic order and Li^+ diffusion.

For example, in the recently reported measurements on $LiMn_2O_4$ where this question was specifically addressed [176], no direct relationship was found between the Li^+ diffusion and magnetism for the Li-Mn-O spinels, although they note that they are tightly connected through the appearance or disappearance of charge order in this material. The muon experiment therefore provide crucial information on the effect of both doping and electronic properties in both magnetism and the Li^+ , resulting in a clear insight regarding how to improve cathode materials.

4. μSR used to study magnetism in organic materials

As has already been shown in the previous section, muons are an extremely effective tool to study magnetism, particularly in relation to their nature as a dynamical and localised probe. They provide complementary information to other more wide-spread techniques, and often unique insight into many materials that traditionally sit within the bounds of magnetism. However, in recent decades, significant interest has been generated in soft materials, and it is only natural that some of this interest involves magnetism. Indeed, in soft matter magnetism, muons are potentially even more useful as probes than in the more traditional magnetic materials discussed above.

4.1. Molecular magnets

The field of molecular magnetism has recently produced many advances via a multitude of new families of materials (see, for example, [177] or [178]). In addition to the transition-metal and lanthanoid based metal-organic complexes, there are also fully organic magnets, containing only the elements carbon, hydrogen, oxygen, and nitrogen. Many organic radicals have unpaired spins, but few have crystalline structures, and even when the spins do align they are rarely ferromagnetic. The structural disorder coupled with the likely dynamics of the unpaired spins makes a localised, dynamic probe of magnetism an essential tool.

The discovery of ferromagnetism in nitronyl nitroxide molecular crystals was quite remarkable, as they are fully organic (and do not contain $d-$ or $f-$ electron atoms, which are normally a prerequisite for ferromagnetism). The first material discovered was para-nitrophenyl nitronyl nitroxide (p-NPNN), which showed ferromagnetism up to $T_c = 0.65$ K in one of its crystal phases [179], as a result of an unpaired spin associated with the two NO groups on each nitrile molecule. Muon experiments on this and other materials in the series began soon after the initial discovery [180, 181, 182, 183, 184, 185].

It was shown that the muons form muonium in the material, which then reacts to the nitronyl nitroxide, forming a muoniated radical. The resulting electronic spin-state of the muonated radical is then either a singlet or a triplet [183]. In the diamagnetic, or singlet, state the muon-spin precesses at a frequency proportional to the local magnetic field at the muon site (with the proportionality constant given by the muon's gyromagnetic ratio). In a paramagnetic, or triplet, state the muon-spin precesses at very high frequency as a result of the hyperfine field, and in principle, this state could be investigated via ALC spectroscopy, although to our knowledge, no such study has been performed to date.

By fitting the temperature dependence of the precession frequency of the muon's spin, it was concluded that the material exhibited three-dimensional long range magnetic order, as it was consistent with a three-dimensional Heisenberg model close

to T_c. At low temperatures the reduction in local field is in good agreement with a Bloch-$T^{3/2}$ law, indicative of three-dimensional spin waves [183]. In 3-quinolyl nitronyl nitroxide (3-QNNN), a reduced local field is observed at the muon site, which is consistent with a canted magnetic structure [180, 184]. In para-pyridyl nitronyl nitroxide (p-PYNN), weak precession below 90 mK is observed, superimposed on a large background [182]. This is as a result of a more complicated magnetic structure, since the molecules are arranged in a one-dimensional chain that favours ferromagnetic interactions along the chain and antiferromagnetic inter-chain interactions.

Whilst the case for muonium formation in the nitronyl nitroxides was clear - a reduced diamagnetic asymmetry - the main probe of the magnetism was the diamagnetic muons. However, as has recently been shown, ALCs are an extremely sensitive probe of spin dynamics in organic materials [52, 47]. It is therefore quite surprising that the only demonstration of ALCs in organic magnets in the literature that we are aware of to date was very recent indeed [186], despite for many years the existence of the high-field spectrometers required to study them.

Another purely organic magnet, discovered some time after the nitronyl nitroxide molecular crystals, is Tanol suberate. This is a biradical, with the formula $(C_{13}H_{23}O_2NO)_2$. The susceptibility follows a Curie-Weiss law with a positive Curie temperature 0.7 K. The specific heat has an anomaly at 0.38 K and is found to be an antiferromagnet [187], but in a field of 6 mT undergoes a metamagnetic transition [188, 189]. Muon measurements yield clear spin precession oscillations [190] and the temperature-dependence of the precession frequency is consistent with a two-dimensional XY magnet [191]. The relaxation rate of the oscillations rises to a maximum at the transition temperature and then falls dramatically. A significant jump in transition temperature was discovered in the β crystal phase of the dithiadiazolyl molecular radical p-$NC(C_6F_4)$(CNSSN) [192], which becomes a non-collinear anti-ferromagnet below 35 K. Zero field μSR has been used to study the internal field in this system [193], where two distinct frequencies are resolved, which have been assigned to muonium bonded at two different sites on the CNSSN ring. The data show that the easy direction for the spin structure is along the b axis and the relaxation rate follows a power law expected for two-magnon scattering. A distinct anti-resonance feature just below the magnetic transition is observed which has been assigned to an interaction between magnons and low-frequency phonons [193].

Some of the most promising materials are molecular magnets that contain a transition metal or lanthanide ion to provide the unpaired electron and organic bridges acting as exchange pathways. One of the first examples of charge transfer magnetic materials is based on TCNQ (7,7,8,8-tetracyanoquinodimethane) as an acceptor and a metallocene as an electron donor, such as $[Fe(Cp^*)_2][TCNQ]$, which produced alternating stacks of electron donors and acceptors where there was no direct bonding between the two. A transition temperature T_c of 2.55 K from a paramagnetic to a metamagnetic phase was obtained from this compound [194, 195, 196]. Another series based on TCNQ is the $M(TCNQ)_2$ series, where M = Fe, Mn, Co and Ni [197]. These new compounds are unsolvated and crystalline. The $Ni(TCNQ)_2$ showed a bulk ferromagnet transition with a $T_C = 20.8$ K; however, it was believed that there is a glassy component associated with the magnetic transition. Muons were used to investigate $Ni(TCNQ)_2$ [198] and the ZF data confirmed that the sample undergoes a bulk ferromagnetic transition at a temperature similar to that observed by the bulk magnetisation data. However, ZF measurements also showed that another transition occurs below 6 K, which is believed to be a transition to a magnetic glassy state. The

LF results indicate that a dynamical component to the magnetism is present below T_c, since LF fields up to 0.45 T cannot completely decouple the spins of the implanted muons from the internal field. Taken together, the ZF and LF results suggest the presence of two dominant sites for implanted muons, one of which is strongly coupled to the bulk magnetic transition and the other that is more weakly coupled and has a dynamical magnetic environment below T_c. This could be as a consequence of muon spin relaxation probing core and surface magnetic environments of nanoparticles or clusters.

Another example is (DMeFc)TCNE where DMeFc = $Fe[(CH_3)5C_5]_2$ is a donor and TCNE is an acceptor, which has a quasi-1D chain structure and exhibits bulk ferromagnetism below 4.8 K [199]. Muons have been used to measure short-range and very slow spin correlations above this temperature [200]. Molecular magnets are also possible using the dicyanamide ligand, such as $Ni(N(CN)_2)_2$ and $Co(N(CN)_2)_2$, which exhibit long-range ferromagnetic order below 21 K and 9 K, respectively. Muon experiments detect magnetic order by a highly damped precession signal below T_c, suggesting a broad internal field distribution [201, 202, 203].

One recent paper on magnetic coordination polymers has investigated a material comprising three building blocks [204]: pyrazine ($N_2C_4H_4$ abbreviated pyz), pyridine-N-oxide (C_5H_5NO, abbreviated pyo) and the bifluoride ion $[(HF_2)^-]$. The first two are planar rings and the last is a linear ion, bound by particularly strong hydrogen bonds F-H-F. In this paper, a systematic study of several families of quasi two-dimensional molecular antiferromagnets with a magnetic metal cations Cu^{2+}, Ag^{2+} and Ni^{2+} is reported. In each case, muons were used to extract the transition temperatures, which are often difficult to unambiguously identify with specific-heat and magnetic-susceptibility measurements. They combined these measurements with predictions of quantum Monte Carlo calculations to identify the extent to which each is a good example of the S = 1/2 two-dimensional square-lattice quantum Heisenberg antiferromagnet model [205]. The parameters derived from the temperature evolution of the muon precession frequencies do not show a strong correlation with the degree of isolation of the 2D magnetic layers. Figure 18 shows some example time spectra and fit parameters of two example compounds.

The authors point out, however, that muons may not always offer relevant information about the molecular magnets. In the molecular systems measured, and similar ones but with a magnetic ion with a larger moment, the precession signal becomes increasingly damped as the moment is increased. Cu^{2+} has the lowest damping rate, followed by Ni^{2+}, but no oscillations were present in Fe and Mn containing molecules [204, 206]. Moreover, the temperature dependence of the relaxation rates appears quite complex, but could in principle, probe critical behaviour above the transition temperature of the magnet. However the unambiguous identification of this behaviour is often problematic. Despite these limitations, the technique still appears uniquely powerful in providing insights into the magnetism of these materials and will certainly be useful in the future as more and more new systems are synthesised.

Muon spin relaxation measurements have recently been reported on dimethylammonium metal formates, $[(CH_3)_2NH_2]M(HCOO)_3$ with M = Ni, Co, Mn, and Cu [207]. These hybrid organic-inorganic materials have a perovskite structure, exhibit weak ferromagnetism and are, apart from the copper system, multiferroics with well-separated magnetic and antiferroelectric transitions. In these materials, T_N decreases as the moment size grows, which indicates that the indirect exchange interaction

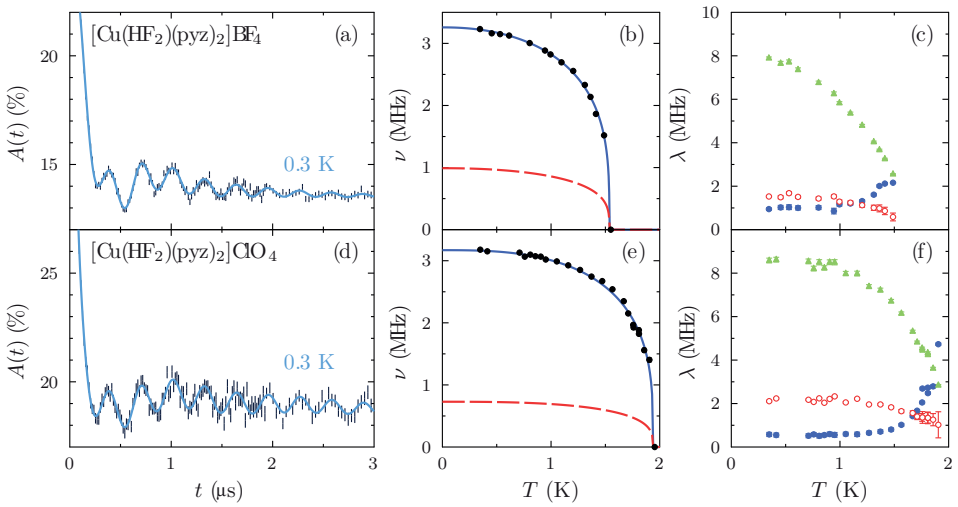

Figure 18: (a) and (d) show sample asymmetry spectra; (b) and (e) frequencies as a function of temperature; (c) and (f) relaxation rates as a function of temperature for $[Cu(HF_2)(pyz)_2]BF_4$ and $[Cu(HF_2)(pyz)_2]ClO_4$ respectively [204].

through the ligands has a greater influence on the ordering temperature than the moment size, similar to a related compound [208]. Moreover, the internal fields do not appear to follow the moment size either, potentially due to the slightly different muon sites or the specifics of the vector sum of dipole moments (from slight changes in the orientation of the spins). The spin-reorientations influence the muon data at higher temperature than in ac susceptibility measurements [209], suggesting they are continuous and associated with a broad range of time scales. The Cu member is found to be quasi-one-dimensional, and the ratio of its inter- and intra-chain exchange constants is $|J'/J| = 0.037$, which is similar to the ratio in $KCuF_3$ where the behaviour is also determined by a Jahn-Teller distortion [210].

μSR has also been recently used as a magnetic probe to study the properties of $Co(hfac)_2$2BPNN (CoBPNN), a one-dimensional cobalt(II)-radical coordination polymer magnet [211]. Preliminary measurements showed that CoBPNN is a hard magnet below 10 K and a soft magnet between 10 K and 45 K. In ZF measurements a Gaussian depolarisation was observed above 60 K. With decreasing temperature a Lorentzian depolarisation was observed together with a decrease of the initial asymmetry, and below 30 K a recovery and very slow exponential depolarisation were observed [211]. The authors conclude that this behaviour is compatible with a static magnetically ordered state, and they define the magnetic transition temperature as 40 K [211]. The very small depolarisation at base temperature indicates that the spins are frozen within the μSR timescale. A coherent muon-spin Larmor precession is observed, that is interpreted in terms of the presence of an appreciable internal magnetic field due to spontaneous magnetisation. The coherency implies that the sample is in a long-range-ordered state [211].

Finally, another class of materials that exhibit interesting properties are the single molecular magnets, which contain a single ion or multiple magnetic ions (from the transition metal or lanthanoid series) surrounded by organic ligands. For example,

muon spin-relaxation measurements are reported on neutral phthalocyaninato lanthanide single-molecule magnets to determine the low-energy levels structure [212]. This was then compared to the low-frequency spin excitations probed by ac susceptibility, where a high temperature thermally activated regime for the spin dynamics and a low-temperature tunnelling regime are found. While in the activated regime the correlation times for the spin fluctuations estimated by ac susceptibility and μSR agree, clear discrepancies are found in the tunnelling regime. In particular, μSR probes a faster dynamics with respect to ac susceptibility, which do not yield a net change in the macroscopic magnetisation probed by ac susceptibility. Another example is zero field muon spin lattice relaxation measurements of a Dysprosium triangle molecular magnet, where a coexistence of static and dynamic internal magnetic fields is observed [213]. Bulk magnetisation and heat capacity measurements show no indication of magnetic ordering, so the static fields observed by μSR are attributed to the slow relaxation of the magnetisation in the ground state of Dy.

4.2. Organic spintronic devices using LEM

Low energy muon spin rotation has recently been used to measure the spin diffusion length in operational organic spin valves [78]. In these devices, the source of the magnetic signal is the injected spin polarised charge carriers from a ferromagnetic electrode, and not the molecules being probed (which are themselves non-magnetic). Indeed, muons are one of the few techniques capable of measuring the spin diffusion length from electrically injected charge carriers and their polarisation relative to the external field in fully operational spin valves. It is possible to measure spin diffusion in single materials via optical pump/probe techniques. Tunnelling-induced luminescence microscopy can also be used, but it is a surface-sensitive technique that cannot probe the polarisation of injected electrons from a buried interface in an operational device. Spin diffusion in organic spintronic devices can also be accessed by measuring the magnetoresistance, but distinguishing between the different sources of spin decoherence in these complex devices is practically very difficult [78]. Furthermore, it requires measurements of the magnetoresistance on a series of devices of different dimensions and there are issues about how the precise growth conditions influence the spin transport in organic materials.

In the LEM experiments, the muon probes the change in the distribution of the magnetisation in the organic transport layer when a spin-polarised current is applied, at specified depths below the buried injection interfaces in the device [78, 79, 214]. The depth-dependence is adjusted by changing the implantation energy of the muons, so both interface and bulk-semiconductor effects can easily be separated in fully functional devices.

Even in zero current, a distribution of fields is observed, due to the external field and the ferromagnetic electrodes, as can be seen in Figure 19. This distribution of fields was observed to be asymmetric, with a pronounced tail towards the high field side, and it was shown to be consistent with a skewed Lorentzian. On applying a voltage, such zero current distribution changes, due to the presence of the spin-polarised current that contributes to the local magnetic field too [78]. Both the peak field and the skewness of the distribution change, showing an enhancement of the local magnetic fields in the organic spacing layer. This change in the distribution of local magnetic field in the presence of a spin polarised current can be seen in Figure 20 [79].

Through a quantitative analysis of the time-resolved data as measured at different

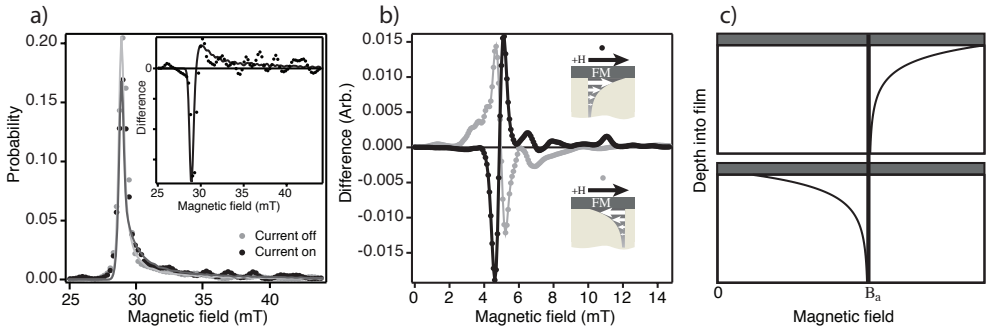

Figure 19: a) The distribution of magnetic fields inside a spin valve at an applied magnetic field of 29 mT. The data with a current density of 0 and 3 mA cm^{-2} are shown in light and dark grey, respectively. The circles show the experimentally measured data that exhibit a small but significant difference between current-on and -off. Inset: The difference between the two data sets (black circles) and the difference predicted by the model (line). b) The difference between the experimentally measured distribution of magnetic fields with the injection current on and off, for an applied field of 5 mT. The black and grey data show different configurations, where the direction of the external field with respect to the spin polarisation of the injected charge carriers is either parallel or antiparallel. It is clear that when in the parallel configuration, the current-on lineshape is skewed to higher magnetic fields, whereas in the antiparallel configuration, the current-on lineshape is skewed to lower magnetic fields. c) Schematic diagram of the two cases shown in b, showing the expected spatial distributions of local magnetic field in the organic layer for both configurations. When the spins of the injected charge carriers are aligned (anti-aligned) with respect to the applied field, the μSR lineshape is skewed to the higher (lower) fields [78].

muon implantation energies, and taking into account the muon stopping profile, the authors can then estimate the spin diffusion length, which they find to be in good agreement with the magnetoresistance measurements. Importantly, the 2009 paper [78] demonstrated bulk spin injection and transport were possible inside organic spin valves, and that it was not pin-hole dominated injection and transport that resulted in the magnetoresistance observed [215].

Following this first proof of principle paper the same technique was used to prove that it is possible to control the polarisation of the charge carriers extracted from an organic semiconductor in a spin valve by inserting a thin polar layer at the interface between the organic and the electrode [79]. To this aim they compared LEM measurements in two spin valves having the same structure, but for a thin interfacial Lithium Fluoride (LiF) layer in one of them. They clearly observe significantly different behaviour in the dependence of the skewness parameter on voltage for the two devices. These differences are accounted for by a reversal of the spin polarisation in the organic semiconductor due to the presence of LiF. In fact, the interface dipole introduced by LiF produces a vacuum level shift, which moves the HOMO energy relative to the Fermi level of the metal contact. As the spin-dependent hole extraction probability depends on the spin polarisation in the cathode at the OSC HOMO energy, a shift in the HOMO would change the spin polarisation of extracted holes. Hence,

this picture explains the differences observed in the LEM data between the two devices with and without LiF.

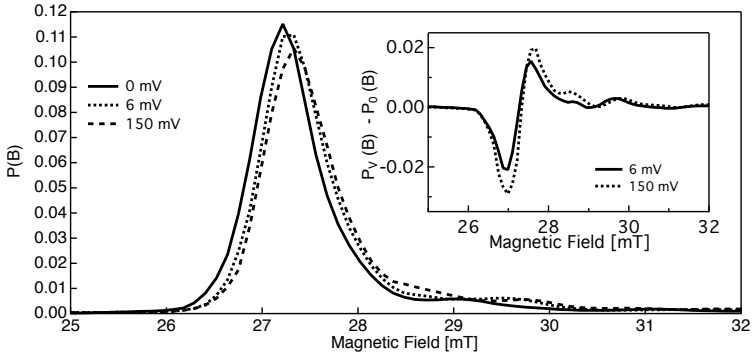

Figure 20: Probability distribution of magnetic field inside an organic spin valve for some selected voltages. The inset shows the difference between spin-polarised current on and off measurements. [79].

5. μSR used to study dynamics in non-magnetic organic materials

As shown by the section on organic spin valves, muons do not necessarily have to reside in a material that is magnetic in order to observe spin dynamics. Indeed, in the case of the electrically operated spin valves discussed above, the molecules where the muons reside are not themselves magnetic, but the presence of mobile spin polarised charge carriers results in a modification of the magnetic environment in which the muons sit. The LEM spin valve measurements discussed above were performed in transverse fields, and the spin polarised charge carriers were detected by a modification of the local magnetic field that the muons observe (via the TF relaxation envelope). However, it is not necessary for the mobile charge carriers to be spin polarised in order to measure their dynamics. Over the last few decades there has been a very active field in measuring the dynamics of unpolarised mobile charge carriers on non-magnetic polymers and other organic systems, by virtue that the muon and electron both have a spin. The electron's motion modulates the hyperfine coupling between it and the muon, resulting in the muon's spin relaxing. These measurements were performed as a function of LF, and the field dependence of the muon's relaxation rate was used to estimate the correlation function of the polaron's motion. Again, the sensitivity to what is essentially spin dynamics makes μSR an extremely powerful probe.

5.1. Polaron motion in polymers

In the majority of conductive conjugated polymers, muonium is formed after muon implantation. Muonium addition to the polymer results in the formation of a negative polaron. This self-doping makes μSR particularly suitable to study materials with a low charge carriers concentration. It has been argued in many papers that the polaron can diffuse along the polymer chain, and occasionally hop to neighbouring chains, with two characteristic and separate diffusion rates, as shown in Figure 21. The fluctuating

spin density due to the rapid motion of the polaron along the chain leads to a relaxation of the muon spin.

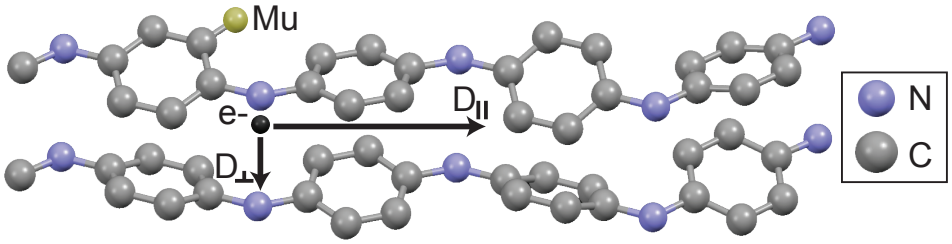

Figure 21: The muoniated radical electron can diffuse along or between the polymeric PANI chains. The motion-induced modulation of the hyperfine interaction coupling between the muon and electron spins gives rise to a muon spin relaxation. From the field dependent relaxation rates, the diffusion constants $D_{||}$ and $D_{\perp}$ can be determined. The crystallographic structure file is from [216]. Hydrogen atoms are not shown for clarity.

The first μSR studies of polymers were performed on trans-polyalanine (trans-PANI), shown in Figure 21, which has the rather unique property of having a ground state with degenerate bond-alternation, and as a consequence allows the formation of free neutral solitons. A field-dependent relaxation was observed shown in Figure 22, interpreted by the presence of mobile solitons. In cis-polyalanine (cis-PANI), which differs from the trans-isomer in that it has no degeneracy in the bond-alternation ground state, a very different behaviour was observed. This also shown in Figure 22; a strong repolarisation effect is seen with very small relaxation [217, 218, 219], as a result of the trapped charge carrier.

Indeed, trans-PA seems to be rather unique in having a degenerate bond-alternation ground state that supports free neutral solitons, and it was not initially clear whether the muon technique would be of use in the more usual non-degenerate systems. In the majority of conducting polymers, which cannot support free solitons, the simplest mobile carriers are charged polarons, which may also move according to the anisotropic diffusion models. A negative polaron is formed which will leave a positive charge if it diffuses away from the muon site, so there is a binding energy to the muon site which may lead to localization of the polaron.

In most polymers, such as trans-PANI♯, polypyridine and polyphenylenevinylene, the experimental data are well fitted by the RK function, and the parameter Γ shows the expected inverse dependence on the field indicating a 1D motion, at least in some temperature and field ranges [220, 221, 222]. In many polymers however a crossover to a field-independent Γ is observed at or close to room temperature, as shown in Figure 23. A departure from the inverse dependence on the applied magnetic field at low fields is observed, indicating that the motion is 3D rather than 1D [221]. The diffusion rate along the chain calculated from Γ in trans-PANI shows a metallic-like behaviour at low temperatures, and above 150 K it becomes inversely proportional

♯ The original experiments [217] on trans-PANI were fit to an exponential function, but it became clear later [221] that the Risch-Kehr formalism that describes 1D stochastic motion of the charge carrier motion may be more appropriate [60].

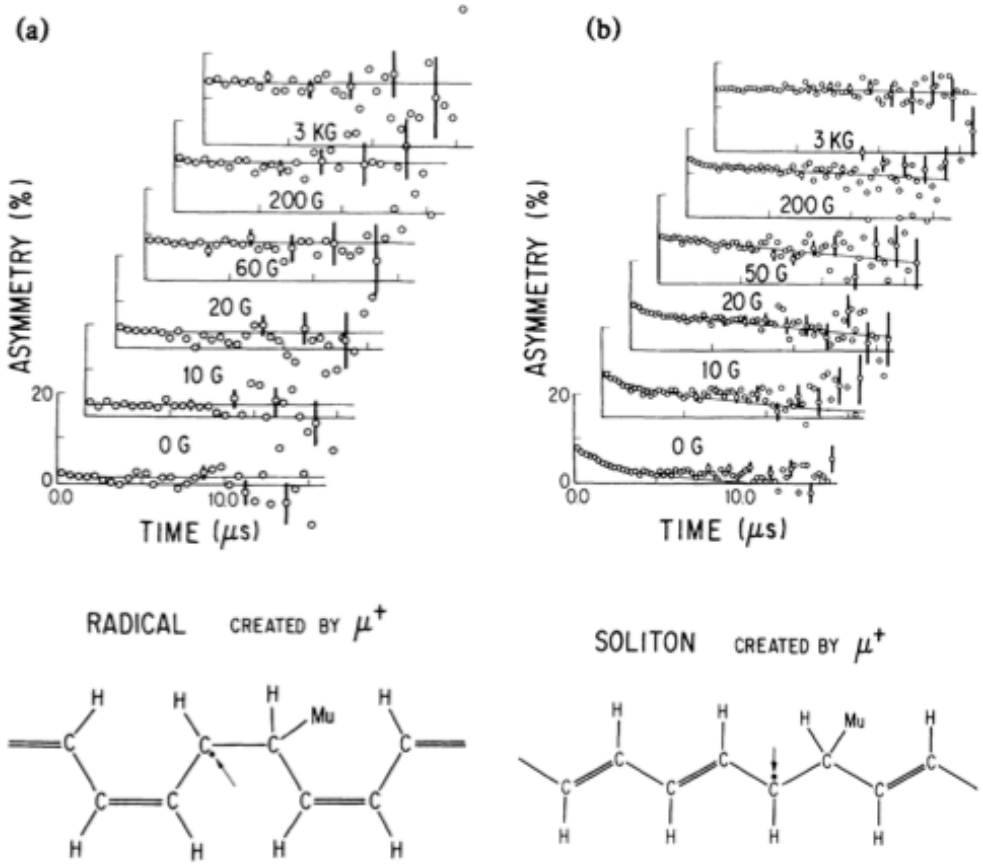

Figure 22: Muon time spectra for (a) cis-PANI and (b) trans-PANI at room temperature for various applied longitudinal fields. The relaxation is much larger for trans-PANI than cis-PANI. The proposed pictures for the muonium states in these two isomers are also shown. [217].

to the temperature, suggesting a phonon-limited metallic transport. On the other hand the interchain diffusion estimated from the cut-off fields shows an activated semiconducting behaviour, and it increases significantly above 150 K. So the phonons assist the interchain diffusion, while they limit the intra-chain motion [220].

It seems that in general, polymers (whether with a degenerate bond-alternating ground state or not) are found experimentally to have a muon spin relaxation behaviour that include both a significant field dependent relaxation that is consistent with the mobile charge carrier models and a repolarising component of the asymmetry that is corresponds to localised electrons [217, 218, 219, 220, 221, 222, 223, 224, 225, 226, 227, 228]. It has been suggested that both localised and mobile spins are present within the same sample [229], but it is not clear the relative importance of the two in their contribution to the muon's spin relaxation. It could also be that it is governed by an entirely localised mechanism that results in similar field and temperature dependencies to the mobile charge carrier models. One possible mechanism that could account for both the relaxation and repolarisation is the spin relaxation of a localised

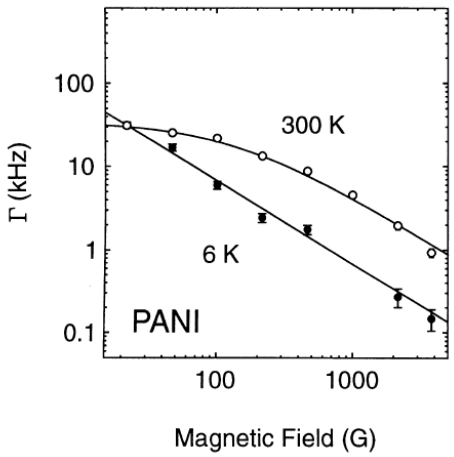

Figure 23: Field dependence of the RK relaxation rate in trans-PANI [221].

muoniated electron. This will be considered below, when discussing small molecules.

5.2. Electron transfer and dynamics in biological systems

Despite the wealth of problems to solve in the biological arena, there has not been the same level of activity in using μSR to probe biophysical systems as there has been in condensed matter physics. This is partly related to the complexity of the problems in biophysics, but could also be down to some degree of self-selection - scientists using muons tend to come from a condensed matter background, and not a biological one. However, there is significant potential for expansion in this direction. For example, the HiFi spectrometer at ISIS is currently being upgraded with a laser, to allow excited states to be measured with muons, with a particular emphasis on biological systems [85].

Analogous to the work on polymer charge carrier dynamics, muons have been used to probe electron transfer processes in a number of biologically relevant molecules, which play a central role in many biological phenomena ranging from enzymes functioning to photosynthesis. For example, μSR measurements have been performed on Cytocrome-C, a protein involved in the respiratory electron transport chain in mitochondria [230, 231, 232]. The relaxation of the muon's spin was observed to depend on the external field, again fitting the data using a Risch-Kehr relaxation function, and the relaxation parameter resulting from these fits is found to decrease monotonically with the applied field. Two regions with different field dependence are observed: a weak dependence at low field and the inverse dependence expected for one-dimensional motion of the electrons in the RK model. The cut-off field is significantly reduced with decreasing temperature. The results are explained in terms of a 1D motion, with the cut-off attributed to an increase in the effective dimensionality of the motion at high temperatures due to an increased inter-chain diffusion rate [230, 231]. The same method has been applied to other proteins, such as ferritin, dextran and

myoglobin [230, 231, 233, 234].

μSR has also been used to study the molecular and electron dynamics in DNA, not only because of the role of electron transfer in the DNA damage and repair mechanisms, but also to elucidate the properties that might make this molecule a candidate for applications in nanotechnology. Electron transfer in DNA at room temperature was reported [235], again using the same method as in polymers, with the data analysed using the RK model. An inverse field dependence of the RK relaxation parameter was observed, suggesting the existence of a rapid 1D diffusion of electrons along the DNA chain [235, 236]. However a comparison of the results at low fields (lower than 80 G) in different DNA conformations shows a difference in the relaxation rate, which was attributed to the different arrangement of the base pairs in the DNA chain. So they concluded that this result is consistent with a picture of electron hopping between base pairs. At temperatures lower than 260 K, a drastic change of the muon spin relaxation rate was observed, interpreted as being due to the onset of glassy dynamics [236]. The RK relaxation function no longer reproduced the experimental data, and it was found that a Kubo-Toyabe function was more appropriate below 160 K. In fields above 1 kG the muon spin relaxation became very small and field independent. The authors interpret all of this behaviour as a suppression of the electron mobility in DNA in the glass phase [236].

5.3. Charge carrier dynamics in small molecules

Muons have also been used to study small molecular semiconductors. Through TF measurements Duarte and coworkers studied the muon states in zinc-phthalocyanine, revealing the existence of two different muoniated radical states, corresponding to the bonding of the muon at two distinct sites on the molecule [238] and a third muon addition site with significant lower hyperfine parameters was identified later on [239]. They observed the onset of a relaxation in LF measurements from 250K, that they attribute to the interaction with charge carriers in the LUMO [238]. They then deepened the investigation on the charge transport in a later work [237], and analysed their data in accordance with the assumption that charge carriers can undergo spin exchange with the electronic spin of the muoniated radical, and that the spin flip rate of this process is proportional to the carrier concentration and velocity. Using an analytical approach that takes into account the polycrystalline nature of the sample, they extract the electronic spin flip rate from the time-dependent LF-μSR measurements [240]. From these measurements, performed as a function of temperature, they also determine the activation energy for the carriers that is significantly lower than the values found from electrical measurements. They assign this discrepancy to a fast component in the conduction in the material studied [237].

In other small molecules, such as Aluminium tris-hydroxyquinolate (Alq_3), it was found that the LF relaxation rate is consistent with the RK model, whereas it was inconsistent with an exponential relaxation. The data and fit for Alq_3 are shown in Figure 24a. As discussed above, the RK model was originally derived to interpret studies on conducting polymers, and it assumes a 1D stochastic charge carrier motion [60]. By fitting the RK relaxation rate as a function of the magnetic field, it was shown that the relaxation rate exhibits the archetypical B^{-1} dependence that the RK model predicts for 1D diffusion, shown in Figure 24b. The authors obtain the intermolecular diffusion constant, and ultimately the electron mobility, from this field dependent relaxation rate. From the cutoff in the magnetic field dependent relaxation

rate, also shown in Figure 24b, they can also derive a limit to the interchain mobility.

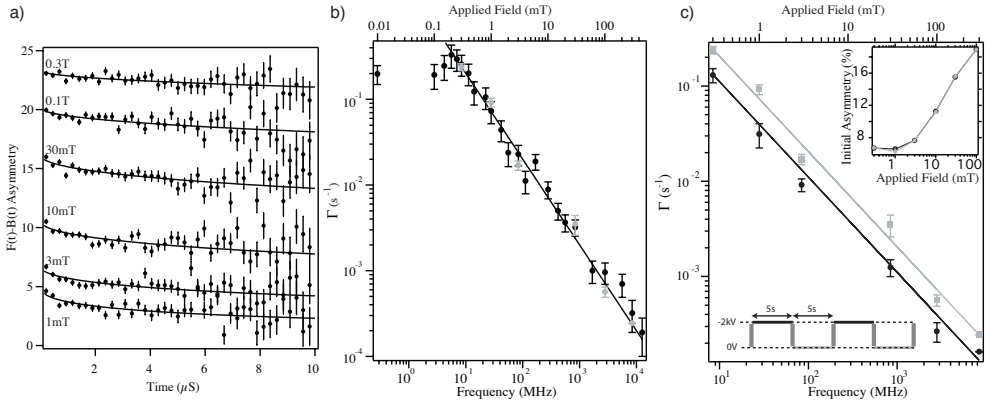

Figure 24: The asymmetry is plotted as a function of time for various external longitudinally applied magnetic fields in Alq_3. The RK model is employed to fit the data and extract the RK relaxation rate. The dependence of RK relaxation rate on the magnetic field (top scale) is shown in b). The proportionality of this RK relaxation to B^{-1} (solid line) is predicted by the RK model for a 1D motion of the electron along the fast direction in the organic material. c) The relaxation rate significantly changes on application of an electric field. [46].

The same approach is used by Saragi and coworkers [241] to investigate another organic semiconductor, 20,70-bis(N,N-diphenylamino)-2-(5-(4-tert-butylphenyl)-1,3,4-oxadiazol-2-yl)-9,9-spirobifluorene (Spiro-DPO). They observe a change in the dependence of the RK relaxation rate on the applied magnetic field as a function of temperature. In particular, as shown in Figure 25, while the data can be fitted by a power law down to low magnetic fields at low temperatures, indicating a 1D hopping of the electrons, this does not hold at room temperature. As a consequence the authors can conclude that a transition from one dimensional hopping to two or three dimensional hopping occurs in this molecule at high temperature [241].

However, recent DFT calculations by McKenzie on the electronic state of the muoniated radicals in Alq_3 have raised questions on the validity of the RK model applied to small molecular semiconductors [242]. Firstly, it was shown that the energy required to transfer an electron between the muoniated radical molecule and a neighbouring molecule depends on the site of addition. Upon calculating the difference in the free energy of the initial (muoniated radical) and final (electron transferred to a neighbouring molecule) states, it was concluded that in all cases electron transfer to a neighbouring molecule is energetically unfavourable. The author then goes on to conclude that the relaxation observed in the LF-μSR spectra of Alq_3 [46] are caused by some mechanism other than electron hopping. Clearly, there are significant discrepancies between theory and experimental data, but also the experimental data itself result in different and possibly contradictory conclusions. Both the DFT calculations and the conclusions of the experimental results shall be critically examined in the following paragraphs.

Firstly, we start by discussing the theory. The electronic state calculated by McKenzie yields the muon-electron hyperfine coupling constants, and comparing them to experimentally derived HF coupling constants is a good indication of the accuracy

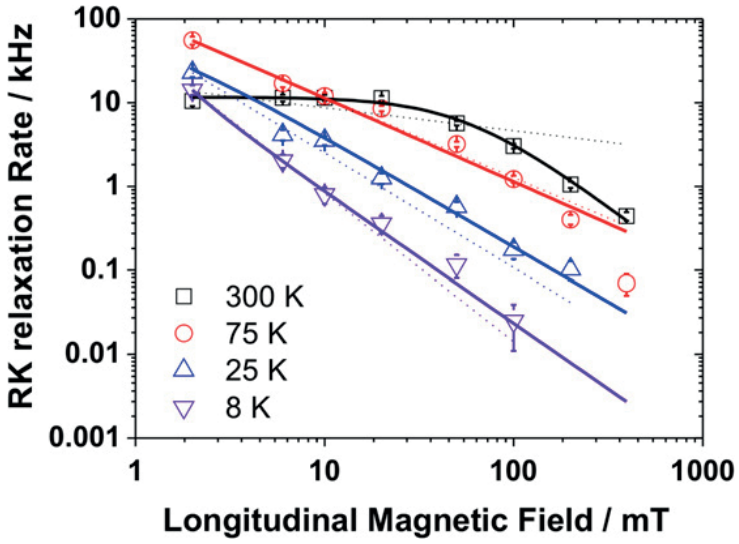

Figure 25: RK Relaxation rate in Spiro-DPO plotted versus longitudinal magnetic field at 8, 25, 75 and 300 K. The solid lines show fits to Farazdaghi-Harris law F(B) = A/(1 + CB^n), with A, C and n are constants. The dotted lines show fits to power law F(B) = CB^n [241].

Site:	A	B	5	7	4	2	3	6
Calculation (MHz)	-	-	224	278	314	343	449	470
Experiment (MHz)	23	91	-	274	311	329	386	420

Table 1: DFT calculated muon-electron HF coupling constants in Alq_3 [242] compared to those obtained from experiments [46, 47]. Sites A and B were not present in the theoretical approach but experimentally shown to exist by means of high-TF field measurements [46]. The remaining HF coupling constants have been experimentally found via the ALC resonance technique [47]. The experimental data has been ordered by increasing HF coupling constants, whereas the theoretical predictions have been matched to the closest experimental value, wherever possible. This may not be correct. For sites 2-7, the numbering convention is from ref [242], as shown in Figure 26.

of the calculations. A comparison is shown in Table 1 and the site assignment in Figure 26. There are two predicted HF coupling constants that are in good agreement with the experimental data (sites 7 and 4) and a third that is relatively close (site 2). However, the remaining predicted HF coupling constants are either not present when there is clear experimental evidence for their existence (sites A and B), or there is a significant difference between predicted and experimental values (Sites 3 and 6). Furthermore, the calculations predict relatively large muon-proton coupling constants (of the order of 100 MHz for some adducts, not shown in Table 1), which would result in a relatively complex set of Δ_0 ALCs, which so far have proved experimentally elusive. Further calculations are necessary to fully understand the muonium states in Alq_3, as these discrepancies with the experimental data indicate the electronic orbitals

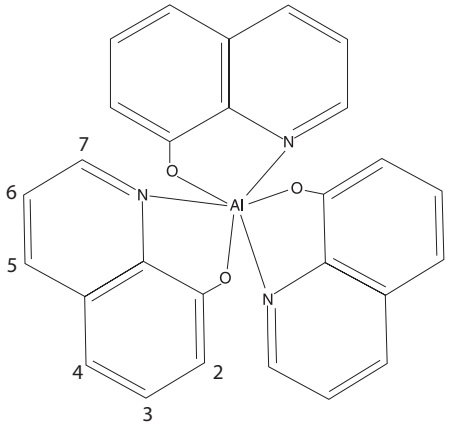

Figure 26: Site assignment used in the DFT calculations by McKenzie [242], for sites 2-7 in Table 1.

calculated are probably different from the ones present in the molecules. This could be related to the isolated molecule approach that was taken, although performing DFT calculations with a realistic crystal structure may prove too challenging; it might be that a hybrid semi-empirical/DFT method may improve the accuracy. Moreover, the calculated difference in the free energy of the initial and final states for electron hopping may need to be revisited, again taking into account a realistic crystal structure may improve this. This is particularly important for the muonium state with the lowest HF coupling, of 21 MHz, which is a very weak coupling constant. It could correspond to either a highly delocalised wavefunction (potentially spreading over more than one molecule) or a weakly coupled muon-electron spin system, resulting from the electron's wavefunction localised to a different ligand or molecule to the muon, and be responsible for the dynamics originally claimed in Alq_3 [46]. Indeed, one of the most compelling sets of evidence that there is some charge carrier dynamics present in the Alq_3 muon measurements is the electric field effect, shown in Figure 24c. The electric field induced reduction in relaxation rate is not a consequence of muonium physics, as the LF repolarisation curves do not indicate any changes on the application of an electric field; it is electronic in its nature [46]. However, it may be related to cloud electrons generated during the muon thermalisation process.

Despite these problems with the calculations, the interpretation of the original experimental work on Alq_3 also needs to be revisited. The presence of several large-amplitude ALCs in Alq_3 [47] and a clear repolarisation curve [46] are indicative of localised electronic states. These experimental data do not point towards dynamical states where the electron is hopping or tunnelling between molecules, which is in qualitative agreement with the DFT calculations. Indeed, as discussed in the next section, the localised muoniated electrons in Alq_3 and several other molecules appear to exhibit significant electron spin relaxation, which could form the major component of the muon's relaxation rate, also in the off-resonance region. Indeed, this may also be true of many of the organic molecules measured so far, including the polymeric systems where similar discrepancies are present in the experimental data.

It seems clear that the measurement of charge carrier dynamics with μSR remains

controversial, particularly for the small molecules. Hopping dynamics should be only observable (or present) in systems with weakly bound muonated radicals, in systems where chargeless solitons can exist. For example, a weakly bound system may be brought about by the extended nature of the wavefunction of the electron and the polarisability of the conjugated electron system, which would both tend to reduce the electrostatic binding potential. Even in the case where the muon-generated polaron is strongly bound to the muon site, it can provide a sensitive probe for the motion of the small concentration of other polarons in these organic semiconductors, that are generally present as a result of impurities or the thermalisation process of the muon in the host material. Nonetheless, it is likely that data in a significant number of the papers discussed here needs to be revisited, with more sophisticated and potentially new models employed to explain the experimental data.

5.4. Electron Spin Relaxation

Spin based electronics (spintronics) is one of the most exciting and challenging areas in modern technologies. It is expected to be of major scientific and social significance that will result in a profound impact on advanced data storage, microelectronics, automotive sensors, quantum computing and biomedical applications. The emerging field of organic spintronics is especially promising for such growing technologies, owing to the long spin coherence times, large flexibility and low production costs of the materials. However, a greater understanding of the fundamental mechanisms behind spin coherence in organic molecules is required to fully utilise their potential. Perhaps most importantly, the relatively long spin coherence time in organic semiconductors has led to significant interest in this class of materials (see, for example, [215]). The ability to measure this key parameter - the spin coherence time - has then become very important in the path towards an optimization of organic spintronic devices, and perhaps more importantly, the fundamental spin physics of these materials, which is still not well defined.

It has been recently demonstrated that μSR, and in particular ALC spectroscopy, can be used to obtain a direct measurement of the intrinsic electron spin relaxation rate in organic semiconductors [52, 243, 47]. This use of μSR has filled in a gap, since the other experimental techniques used previously, such as magnetotransport measurements, had to rely on a theoretical model to extract the electron spin relaxation rate. Importantly, these models were initially developed for conventional band-transport materials, and it is not immediately clear if they are applicable to materials where charge carrier transport is dominated by a hopping process between discrete localised states [244].

As discussed earlier, in organic materials where there is a high fraction of muonium, ALC resonances are observed at field values related to the hyperfine coupling constant. As has recently been shown, the change in amplitude of these ALC resonances is roughly proportional to the electron spin relaxation rate [52, 243, 47]. Shown in Figure 27a is an example of the increase in amplitude of the ALC resonance in TIPS-Pentacene, from which it was relatively straight-forward to extract the electron spin relaxation rate (the mathematics for this is shown in Section 2.3: equations 49 - 51); indeed, the lines shown in Figure 27a are the result of the modelling, from which the electron spin relaxation rate value (0.76 MHz at room temperature) was obtained [52]. The effect of the temperature-dependent electron spin relaxation can also be observed in the time-dependent muon spin relaxation

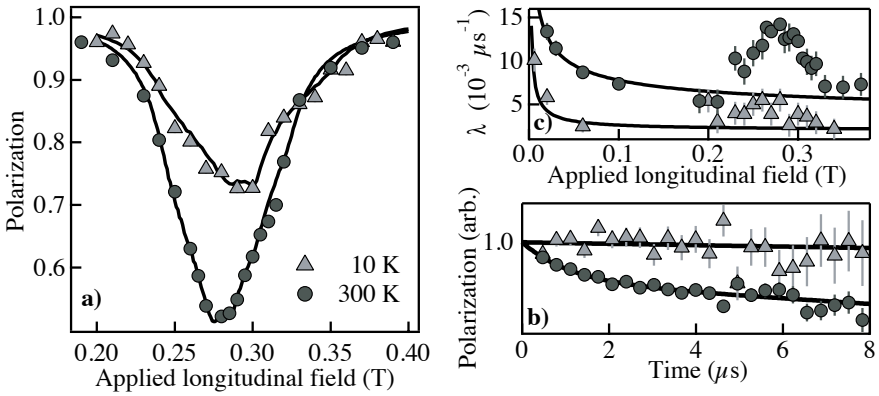

Figure 27: Muon data for TIPS-pentacene for T = 300 K (circles) and T = 10 K (triangles). (a) The muon spin polarisation around the avoided level crossings (ALC). Modelling for these ALCs is indicated by the black lines. (b) The time-dependent muon polarisation at 0.27 T. The black lines correspond to fits to an exponential function, from which the relaxation rate shown in (c) is extracted. (c) The fitted field-dependent exponential muon spin relaxation rate showing that there is a peak in the muon spin relaxation rate around the position of the ALCs. The lines represent the expected power-law dependence for the off-resonant relaxation rate [52].

data, where the muon's spin relaxation rate becomes larger at higher temperatures (See Figure 27b and c) [52]. This effect is amplified around the resonance field, where there is a significant peak in the muon spin relaxation rate as the magnetic field is scanned through the ALC, but still very much present in the off-resonance data (Figure 27b). Could electron spin relaxation be the major part of the muon spin relaxation rate, which was previously attributed to charge carrier dynamics [46, 217, 218, 219, 220, 221, 222, 223, 224, 225, 226, 227, 228, 237, 241]? Indeed, this open question is currently being thought about.

Muons have demonstrated the existence in this class of materials of an intramolecular, temperature-dependent electron spin relaxation mechanism, that had previously been overlooked. This localised mechanism is in contrast with previously reported models based on charge transport only [52]. But, it is worth noting that these measurements in TIPS-Pentacene, even those off-resonance, were performed at relatively high magnetic fields, much more than the few mT required to decouple the proton(s) and electron in these materials. From where does this electron spin relaxation originate?

Given that there are very few restrictions on the type of molecules that can be studied††, it is possible to measure a series of molecules where small chemical, structural or molecular conformational changes are made. This methodology was used to evaluate the role of spin-orbit coupling in the spin relaxation process in organic materials, an interaction that was somewhat neglected by the organic spintronics community. It was commonly assumed in the literature that spin-orbit interaction could not affect the electron spin in these materials due to the low atomic numbers

†† The main restriction being the organic semiconductor must have double/triple bonds or aromatic rings; most do.

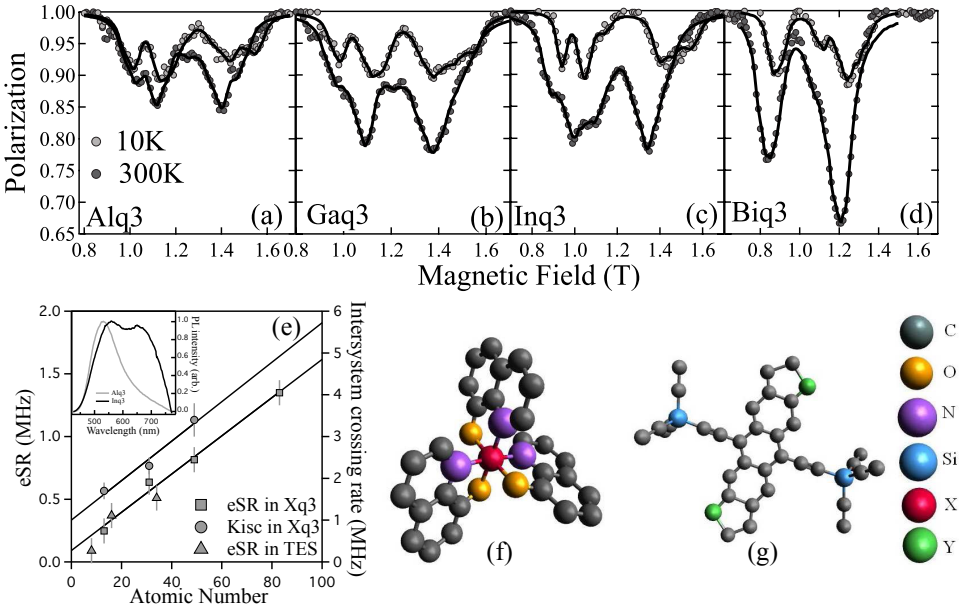

Figure 28: Muon spin polarisation around the ALCs in the Xq_3 series, where X = Al, Ga, In, Bi: (a) Alq_3, (b) Gaq_3, (c) Inq_3, and (d) Biq_3 at 10 K (light grey) and 300 K (dark grey). Modelling for these ALCs is indicated by the black lines and is used to determine the electron spin relaxation rate, which is essentially proportional to the amplitude of the ALC curves [47]. (e) eSR for the Xq_3 and TES series as a function of the atomic number of the substituent atom, Z. Also shown is a measure of the intersystem crossing rate of photo-generated excitons, which shows the same trend and magnitude as the muon results. The inset shows the photo-generated fluorescence and phosphorescence of Alq_3 and Inq_3; there would be no phosphorescence without a high interested crossing rate. Molecular structures of (f) the Xq_3 series, where X = Al, Ga, In, Bi, and (g) the TES series, where Y = O, S, Se. Hydrogen atoms are not shown for clarity.

of their constituent atoms, and that the relaxation was instead due to hyperfine interaction [245, 246]. In a recent paper [47] μSR has been used to assess the role of spin-orbit coupling, by performing targeted chemical substitutions in two series of molecules, to obtain molecules with the same structure but different spin-orbit coupling. One of these series is the tris-hydroxyquinolate (Xq_3) (where the metal is substituted: Aluminium, Gallium, Indium and Bismuth; see Figure 28). The other is the triethylsilylethynyl (TES) series (similar to TIPS-Pentacene, but where an atom on the central backbone is replaced with Oxygen, Sulphur and Selenium: triethylsilylethynyl anthradifuran, triethylsilylethynyl anthradithiophene, and triethylsilylethynyl anthradiselenophene, respectively). μSR was used to estimate the electron spin relaxation rates at room temperature as a function of the substitution. While the amplitude of the ALC curves at 10 K is approximately the same in all the samples within a series, the amplitudes at 300 K increase visibly with the atomic

number of the substituted atoms. The electron spin relaxation rate extracted from the modelling of the ALCs were found to be proportional to the estimate of the spin-orbit coupling, which itself is proportional to the mass of the substituted atom, as shown in Figure 28. This result proves that, differently from what was assumed in the literature, spin-orbit coupling also plays a role in the electron spin relaxation mechanism in organic semiconductors [47].

However, one must be aware that the muoniated radical sits in a different orbital to any unpaired electrons or holes in the HOMO or LUMO, and this might modify the coupling to their environment. As a consequence, it's essential to perform additional measurements that don't involve muons. Nuccio et al. performed time resolved photoluminescence measurements of the Xq_3 series to extract the exciton intersystem crossing rate [47]. Singlet excitons that are generated by the absorption of light have a typical lifetime of ∼10 ns in organic semiconductors, with the primary energy loss mechanism being fluorescence. In systems with a high intersystem crossing rate, the singlet excitons convert into long-lived triplet excitons (often with lifetimes of μs or more). These long-lived triplet excitons can then back-transfer to a singlet which results in delayed fluorescence or direct phosphorescence to the ground state, emitting a different wavelength of light. Indeed, clear phosphorescence in the Xq_3 series is readily observed as the atomic number of the central atom is increased, as demonstrated in the inset to Figure 28e, which clearly demonstrates the importance of the Spin Orbit interaction [47]. Moreover, by fitting the photoluminescence (in particular, the delayed fluorescence) to the relevant rate equations, Nuccio et al. extracted the intersystem crossing rate as a function of atomic number of the substituent atom. This is plotted in the main panel of Figure 28e, where it is clear that the same trend is observed for both the muoniated radical and the intersystem crossing rate. It is also worth noting that there is a significant change in the magnetoresistance of organic light emitting diode devices in the Xq_3 series [247], suggesting that Spin Orbit interaction is relevant in the devices. It must be noted that one must be careful with the absolute values to eSR in small molecular semiconductors, as the muoniated radical electron sits in a somewhat different orbital to the free charge carriers in devices. However, the fact that the value of eSR extracted by muons is similar the values extracted by other techniques, and the trends are the same, clearly informs us that the technique has a lot to offer in unravelling the physics of eSR in molecular semiconductors, not least because there are few materials in this class in which measurements cannot be made.

5.5. Structural dynamics in polymers

Besides the nature of the charge transfer, μSR can also be used to study other properties of polymers or related materials. As an example, non-conductive polymers such as polybutadiene have been studied to understand polymer structural dynamics. In this case, where the muonium radical is highly localised, it is argued that the main contribution to the muon's spin relaxation is the modulation of the hyperfine coupling due to the polymer motion [248], rather than the modulation of spin density associated to the polaron motion as in conducting polymers. Polybutadiene has as consequence been used as a model system to study the glass transition. Both the signal in the TF measurements and the Δ_0 ALC resonance show a broadening on approaching the glass transition temperature, due to the polymer dynamics slowing down [248]. An even clearer effect is observed in LF measurements: a sudden drop in the relaxation

rate is observed at the glass transition temperature [248]. A change in the relaxation rate at the glass transition temperature is also observed in other materials, such as polystyrene. Polystyrene has been studied not only in the bulk form, but also in thin films, using low energy muons [249]. When measuring with low energy muons close to the surface of the sample at a temperature of 5 K below the bulk glass transition temperature, a significantly lower relaxation is observed compared to the bulk at the same temperature. This is interpreted as a reduced glass transition temperature in the surface region [249]. Furthermore, by varying the implantation energy of the low energy muons the authors found out that the bulk behaviour extends to about 35 nm from the surface [249].

6. Conclusion

The examples given in this review demonstrate the broad range of applications of μSR to condensed matter research. Whilst this article emphasises spin dynamics, particularly in magnetic materials, it is clear that there are many more materials and problems that can be investigated with muons that are outside the scope of this review. Whilst muons could be thought of as a rather expensive magnetometer, reporting on internal fields, local spin structures and spin dynamics, their true value is much more than this. One of the most important distinctions of the technique is that it is a local probe, from interstitial rather than substitutional sites. It complements the standard magnetic techniques, such as susceptibility measurements and neutron scattering, and other resonant techniques, such a NMR and eSR. Muons are able to access unusual components of the correlation functions in a wide variety of materials and therefore offer invaluable information. Clearly, muons will continue to be used as probes of magnetic materials, especially those where dynamics are important or those where quantum effects are evident. Moreover, magnetic materials and their phase transitions have provided, and will likely to continue to provide, very convenient systems in which to test statistical mechanics and muons have shown to be an extremely competent way of measuring them.

However, the muon when applied to magnetic materials is often considered to be a passive spin probe. As has been discussed above, muons are also an effective active spin probe of materials - the principal participant in the phenomenon of interest being muonium. However, perhaps more work is needed to fully understand the physics of muonium in soft matter. In particular, it has been argued that there is evidence for a mobile muonium-generated charge carrier in a wide variety of polymers, small molecules and biological systems, despite strong indications that the electron in question is highly localised. Despite the large-body of work carried out over the last few decades, it seems very clear that further experimental and theoretical work is needed to understand and interpret the measured relaxation rates, from which much of the information about charge carrier dynamics is obtained. For example, there appears to be still much to do to evaluate the changes in local electronic structure produced by the addition of the muon to the molecule. On the experimental side, the interpretation of the repolarising asymmetry (thought to be due to a fraction of localized states) is also not entirely certain, although the recent high-field ALC studies of small molecules may offer the desired insight.

Importantly, if these issues around interpretation of muonium in soft-matter systems are resolved, the μSR method can in principle be extended to the study of proteins or DNA in various chemical and biological environments. It has even

been suggested that the muon method could be applied to proteins or DNA in vivo, and possibly even use it to study aspects of electron transfer in active brain tissue [31]. Perhaps more realistically, in the near future, developments in this relatively neglected field of application of μSR include gaining a better understanding of the muoniated radical states in biomacromolecules (also true for small molecules), moving the experiments to better approximations of the physiological conditions (for example, solution experiments in water of the correct pH) and the application of light to create excited states [85].

7. Acknowledgements

Leander Schulz would like to acknowledge financial support from the Swiss National Science Foundation, grant numbers PBFRP2-138632 and PBFRP2-142820. Alan Drew would like to acknowledge financial support from the UK Engineering and Physical Sciences Research Council, grant number EP/G054568/1, the European Union Seventh Framework Programme project NMP3-SL-2011-263104 "HINTS" and the European Research Council project "Muon Spectroscopy of Excited States (MuSES)". Alan Drew would also like to thank Iain McKenzie, James Lord and Francis Pratt for the insightful discussions about many of the current issues presented here.

References

[1] Nagamine K et al. 2004 *Proc. Jpn. Acad. Ser B* **80** 179
[2] Miyadera H et al. 2013 *AIP Advances* **3** 052133
[3] Michida S et al. 2012 *Nat. Phys.* **8** 243
[4] Patterson B 1988 *Rev. Mod. Phys.* **60** 69
[5] Blundell S J 1999 *Contemp. Phys.* **40** 175
[6] Nagamine K 2007 *Introductory Muon Science* Cambridge University Press
[7] Schenck A 1985 *Muon Spin Rotation Spectroscopy: Principles and Applications in Solid State Physics* Adam Hilger Ltd.
[8] Yaouanc A and Dalmas de Réotier P 2011 *Muon Spin Rotation, Relaxation and Resonance* Oxford Science Publications
[9] Blundell S J 2004 *Chem. Rev.* **104** 5717
[10] Lee S L, Kilcoyne S H, Cywinski R 1999 *Muon Science. Scottish Universities Summer School in Physics*, IOPP (Bristol)
[11] Heffner R H and Nagamine K 2004 *J. Phys.: Cond. Matt.* **16** (Special issue on μSR)
[12] Amato A et al. 2004 *J. Phys.: Cond. Matt.* **16** S4403
[13] Kadano R 2004 *J. Phys.: Cond. Matt.* **16** S4421
[14] Khasanov R et al. 2004 *J. Phys.: Cond. Matt.* **16** S4439
[15] Klauss H 2004 *J. Phys.: Cond. Matt.* **16** S4457
[16] MacLaughlin D E et al. 2004 *J. Phys.: Cond. Matt.* **16** S4479
[17] Sonier J E 2004 *J. Phys.: Cond. Matt.* **16** S4499
[18] Uemura Y J 2004 *J. Phys.: Cond. Matt.* **16** S4515
[19] Heffner R H, MacLaughlin D E, Nieuwenhuys G J and Sonier J E 2004 *J. Phys.: Cond. Matt.* **16** S4541
[20] Lancaster T et al. 2004 *J. Phys.: Cond. Matt.* **16** S4563
[21] Morenzoni E et al. 2004 *J. Phys.: Cond. Matt.* **16** S4583
[22] Keren A 2004 *J. Phys.: Cond. Matt.* **16** S4603
[23] Ryan D H, van Lierop J and Cadogan J M 2004 *J. Phys.: Cond. Matt.* **16** S4619
[24] Schenk A and Solt G 2004 *J. Phys.: Cond. Matt.* **16** S4639
[25] Dalmas de Réotier P, Gubbens P C M and Yaouanc A 2004 *J. Phys.: Cond. Matt.* **16** S4687
[26] Lord J S et al. 2004 *J. Phys.: Cond. Matt.* **16** S4707
[27] Lichti R L et al. 2004 *J. Phys.: Cond. Matt.* **16** S4721
[28] Lord J S et al. 2004 *J. Phys.: Cond. Matt.* **16** S4739

[29] Storchak V G, Eshchenko D G and Brewer J H 2004 *J. Phys.: Cond. Matt.* **16** S4761
[30] Pratt F L 2004 *J. Phys.: Cond. Matt.* **16** S4779
[31] Nagamine K and Torikai E 2004 *J. Phys.: Cond. Matt.* **16** S4797
[32] Cox S F J 2009 *Rep. Prog. Phys.* **72** 116501
[33] Cox S F J 2002 et al., *J. Phys. D: Appl. Phys.* **35** 586
[34] Sonier J E 2010 *J. Phys. Cond. Matt.* **22** 203202
[35] Sonier J E 2007 *Rep. Prog. Phys.* **70** 1717
[36] Sonier J E et al. 2000 *Rev. Mod. Phys.* **72** 769
[37] Cohen J S 2004 *Rep. Prog. Phys.* **67** 1769
[38] Sathayanarayana D N 2009 *Introduction to Magnetic Resonance Spectroscopy ESR, NMR, NQR* IK International Publishing House
[39] Kubo R and Toyabe T 1967 *Magnetic Resonance and Relaxation* Ed. by R. Blinc (North Holland, Amsterdam)
[40] Hayano R S et al. 1979 *Phys. Rev. B* **20** 850
[41] Dalmas de Réotier P and Yaouanc A 1992 *J. Phys. Cond. Matt.* **4** 4533
[42] Pratt F L 2007*J. Phys. Cond. Matt.* **19** 456207
[43] Heffner R H et al. 2000 *Phys. Rev. Lett.* **85** 3285
[44] Schneider J W 1989 PhD thesis (Univ. Zurich), *Avoided Level Crossings: A New Technique in Muon Spin Rotation to Study the Nuclear Hyperfine Structure of Muonium Centres in Semiconductors*
[45] Pratt F L 1997 *Phil. Mag. Lett.* **75** 371
[46] Drew A J et al. 2008 *Phys. Rev. Lett.* **100** 116601.
[47] Nuccio L et al. 2013 *Phys. Rev. Lett.* **110** 216602
[48] Roduner E 1993 *Chem. Soc. Rev.* **22** 337
[49] Roduner E et al. 1998 *J. Phys. Chem. A* **102** 7591
[50] Fleming F G et al. 2002 *J. Phys. Chem. B* **106** 6395
[51] Bridges M D et al. 2007 *J. Phys. Chem. C* **111** 9779
[52] Schulz L et al. 2011 *Phys. Rev. B*, **84** 085209
[53] Roduner E et al. 1995 *Chem. Phys.* **192** 231
[54] Meier P F, 1982 *Phys. Rev. A* **25** 1287
[55] Heming M et al. 1986 *Hyp. Int.* **32** 727
[56] Devreux F, Boucher J P and Nechtschein M 1974 *J. Physique* **35** 19
[57] Butler M A, Walker L R and Soos Z G 1976 *J. Chem. Phys.* **64** 3592
[58] Mizoguchi K 1990 *Makromol. Chem. Makromol. Symp.* **37** 53
[59] Mizoguchi K and Kume K 1993 *Sol. Stat. Commun.* **89** 971
[60] Risch R and Kehr K W 1992 *Phys. Rev. B* **46** 5246.
[61] S. R. Keitzman et al. 1995 *Chem. Phys.* **192** 189
[62] Morenzoni E M et al. 1994 *Phys. Rev. Lett.* **72** 2793
[63] Harshman D R et al. 1987 *Phys. Rev. B* **36** 8850
[64] Morenzoni E M et al. 2003 *Physica B* **326** 196
[65] Prokscha T et al. 2008 *Nucl. Inst. Meth. A* **595** 317
[66] Morenzoni E M et al. 2009 *Physica B* **404** 577
[67] Nagamine K et al. 1995 *Phys. Rev. Lett.* **74** 4811
[68] Iwasaki M and Ishida K 2010 *J. Phys. Conf. Ser.* **225** 012005
[69] Bakule P et al. 2008 *Nucl. Inst. Meth. B* **335** 266
[70] Morenzoni E M et al. 2011 *Nat. Com.* **2** 272
[71] Suter A et al. 2011 *Phys. Rev. Lett.* **106** 237003
[72] Charnukha A et al. 2012 *Phys. Rev. Lett.* **109** 017003
[73] Dunsiger S et al. 2010 *Nat. Mat.* **9** 299
[74] Dean M P M et al. 2012 *Nat. Mat.* **11** 850
[75] Morenzoni E et al. 2008 *Phys. Rev. Lett.* **100** 147205
[76] Prokscha T et al. 2007 *Phys. Rev. Lett.* **98** 227401
[77] Antognini A et al. 2012 *Phys. Rev. Lett.* **108** 143401
[78] Drew A J et al. 2009 *Nat. Mat.*, **8** 109
[79] Schulz L et al. 2011 *Nat. Mat.*, **10** 39
[80] Cottrell S P et al., 2000 *Physica B* **289** 69
[81] Krasnoperov E et al. 1994 *Hyp. Int.* **87** 1011
[82] Storchak V G et al. 1995 *Phys. Rev. Lett.* **75** 2384
[83] Jayasooriya U A et al. 2004 *Chem. Phys. Chem.* **5** 257
[84] Bakule P et al. 2012 *J. Phys. Chem. Lett.* **3** 2755
[85] Yokoyama K et al. 2013 *Phys. Scr.* **88** 068511

[86] http://muses.ph.qmul.ac.uk/
[87] De Renzi R et al. 1994 *Phys. Rev. B* **30** 197
[88] Uemura Y J 1986 *Hyp. Int.* **31** 313
[89] Yaouanc A et al. 1993 *Europhys. Lett.* **21** 93
[90] Yaouanc A et al. 1993 *Phys. Rev. B* **47** 796
[91] Dalmas de Réotier P 1994 et al *Phys. Rev. B* **50** 3033
[92] Heffner R et al. 1996 *Phys. Rev. Lett.* **77** 1869
[93] Garcia-Munoz J L et al. 1999 *J. Appl. Phys.* **85** 5639
[94] Barsov S G 2000 *Physica B* **289-290** 81
[95] De Teresa J M 2002 *Phys. Rev. B* **65** 100403
[96] Yaouanc A et al. 1996 *Phys. Rev. B* **53** 350
[97] M. Mulders A M et al. 2003 *Phys. Rev. B* **67** 014303
[98] I Halperin B I and Hohenberg P C 1967 *Phys. Rev. Lett.* **19** 700
[99] Ishida K et al. 2003 *Phys. Rev. B* **68** 184401
[100] Hillier A D et al. 2007 *Phys. Rev. B* **76** 174439
[101] Adroja D T et al. 2008 *Phys. Rev. B* **78** 014412
[102] Lausberg S et al. 2012 *Phys. Rev. Lett.* **109** 216402
[103] Egetenmeyer N et al. 2012 *Phys. Rev. Lett.* **108** 177204
[104] Canella V et al. 1971 *J. Appl. Phys.* **42** 1689
[105] Anderson P W 1970 *Mat. Res. Bull.* **5** 549
[106] Murnick D E et al. 1976 *Phys. Rev. Lett.* **36** 100
[107] Heffner R et al. 1982 *J. Appl. Phys.* **53** 2174
[108] MacLauchlin D E et al. 1983 *Phys. Rev. Lett.* **51** 927
[109] Uemura Y J et al. 1985 *Phys. Rev. B* **31** 546
[110] Hennion B et al. 1984 *J. Phys. F* **14** 489
[111] Hennion B et al. 1986 *Physica B* **49** 136
[112] Barsov S G et al 1994 *Hyp. Int.* **85** 357
[113] Mirebeau I et al. 1997 *Hyp. Int.* **104** 343
[114] Campbell I A and Bernardi L 1994 *Phys. Rev. B* **49** 729
[115] Cywinski R and Rainford B D 1994 *Hyp. Int.* **85** 215
[116] Dunsiger S R et al. 1996 *Phys. Rev. B* **54** 0919
[117] Telling M T F et al. 1998 *J. Mag. Mag. Mat.* **177** 1480
[118] Sagi E et al. 2005 *Phys. Rev. Lett.* **94** 237202
[119] Stewart J R et al. 1998 *J. Mag. Mag. Mat.* **177** 602
[120] Pinkvos H et al. 1990 *Phys. Rev. B* **41** 590
[121] Komori T et al. 1995 *J. Phys. Soc. Jap.* **64** 4418
[122] Keren A et al. 1996 *Phys. Rev. Lett.* **77** 1386
[123] Keren A et al. 2002 *Phys. Rev. Lett.* **89** 107201
[124] Jonsson P E et al. 2007 *Phys. Rev. Lett.* **98** 256403
[125] Ancona-Torres C et al. 2008 *Phys. Rev. Lett.* **101** 057201
[126] Wenhao Wu et al. 1993 *Phys. Rev. Lett.* **71** 1919
[127] Tam K M and Gingras M J P 2009 *Phys. Rev. Lett.* **103** 087202
[128] Rodriguez J et al. 2010 *Phys. Rev. Lett.* **105** 107203
[129] Taira N et al 2001 *J. Phys.: Cond. Mat.* **13** 5527
[130] Zhao S et al. 2011 *Phys. Rev. B* **83** 180402
[131] Yaouanc A, Maisuradze A and Dalmas de Réotier P 2013 *Phys. Rev. B* **87** 134405
[132] Gardner J S et al. 1999 *Phys. Rev. Lett.* **82** 1012
[133] Hodges J A et al. 2002 *Phys. Rev. Lett.* **88** 077204
[134] Dunsiger S R et al. 2000 *Phys. Rev. Lett.* **85** 3503
[135] Yaouanc A et al. 2005 *Phys. Rev. Lett.* **95** 047203
[136] Bert F et al. 2006 *Phys. Rev. Lett.* **97** 117203
[137] Dalmas de Réotier P et al. 2006 *Phys. Rev. Lett.* **96** 127202
[138] Storchak V G et al. 2010 *Phys. Rev. Lett.* **105** 076402
[139] Bobo D et al. 2004 *Phys. Rev. Lett.* **93** 187201
[140] Pratt F L et al. 2012 *Nature* **471** 612
[141] Anderson P W 1973 *Materials Research Bulletin* **8** 153
[142] Balents L 2010 *Nature* **464** 199
[143] Kanada M et al. 1999 *J. Phys. Soc. Jap.* **68** 3802
[144] Yaouanc A et al. 2011 *Phys. Rev. B* **84** 184403
[145] Kermarrec E et al. 2011 *Phys. Rev. B* **84** 100401
[146] Clark L et al. 2013 *Phys. Rev. Lett.* **110** 207208

[147] Bramwell S T et al. 2009 *Nature* **461** 956
[148] Castelnovo C, Moessner, R. and Sondhi S L 2008 *Nature* **451** 42
[149] Onsager L 1934 *J. Chem. Phys.* **2** 599
[150] Dunsiger S R et al. 2011 *Phys. Rev. Lett.* **107** 207207
[151] Blundell S J 2012 *Phys. Rev. Lett.* **108** 147601
[152] Quemerais P et al. 2012 *Phys. Rev. Lett.* **109** 127601
[153] Lago J, Blundell S J and Baines C 2007 *J. Phys.: Cond. Mat.* **19** 326210
[154] Chang L J et al. 2013 *Scient. Rep.* **3** 1881
[155] Bramwell S T and Giblin S R, Comment on Spin ice: magnetic excitations without monopole signature using μSR (arXiv:1110.0877), arXiv:1111.4168.
[156] Rodriguez J A et al. 2013 *Phys. Rev. B* **87** 184427
[157] Potashnik S J et al. 2001 *Appl. Phys. Lett.* **79** 1495
[158] Jungwirth T et al. 2005 *Phys. Rev. B* **72** 165203
[159] Hamaya K et al. 2005 *Phys. Rev. Lett.* **94** 147203
[160] Uemura Y J et al. 2007 *Nat. Phys.* **3** 29
[161] Storchak V G et al. 2008 *Phys. Rev. Lett.* **101** 027202
[162] von Molnar S and Methfessel S 1967 *J. Appl. Phys.* **38** 959
[163] Methfessel S and Mattis D C 1972 *Magnetic Semiconductors* edited by S. V. Vonsovskii (Mir, Moscow)
[164] Petrich G, von Molnar S and Penny T 1971 *Phys. Rev. Lett.* **26** 885
[165] Storchak V G et al. 2009 *Phys. Rev. B* **80** 235203
[166] Kiefl R F 2011 *Phys. Rev. B* **83** 077201
[167] Storchak V G et al. 2011 *Phys. Rev. B* **80** 077202
[168] Monteiro P M S et al. 2013 *Phys. Rev. Lett.* **110** 217208
[169] Kaiser C T et al. 2000 *Phys. Rev. B* **63** R9236
[170] Sugiyama J et al. 2009 *Phys. Rev. B* **79** 184411
[171] Sugiyama J et al. 2010 *Phys. Rev. B* **82** 224412
[172] Sugiyama J et al. 2009 *Phys. Rev. Lett.* **103** 147601
[173] Sugiyama J et al. 2008 *Phys. Rev. B* **78** 144412
[174] Nozaki H et al. 2013 *J. Phys.: Cond. Mat.* **25** 286005
[175] Sugiyama J et al. 2011 *Phys. Rev. B* **84** 054430
[176] Kamazawa K et al. 2011 *Phys. Rev. B* **83** 094401
[177] Kahn O 1993 *Molecular Magnetism* VCH.
[178] Blundell S J and Pratt F L 2004 *J. Phys.: Condens. Mat.* **16** R771
[179] Tamura M et al. 1991 *Chem. Phys. Lett.* **186** 401
[180] Pratt F L et al. 1993 *Synth. Met.* **61** 171
[181] Le L P et al. 1993 *Chem. Phys. Lett.* **206** 405
[182] Blundell S J 1994 et al. *Sol. Stat. Commun.* **92** 569
[183] Blundell S J 1995 et al. *Europhys. Lett.* **31** 573
[184] Blundell S J 1997 *Hyp. Int.* **104** 251
[185] Zheludev A et al. 1994 *Sol. State. Com.* **90** 233
[186] Lancaster T et al. 2011 *J. Phys.: Cond. Mat.* **23** 242201
[187] Saint Paul M and Veyret C 1973 *Phys .Lett.* **45A** 362
[188] Benoit A et al. 1983 *J. Mag. Mag. Mat.* **31-34** 1155
[189] Chouteau G and Veyret-Jeandey C I 1981 *J. Physique* **42** 1441
[190] Sugano T et al. 1999 *Molecular Crystals and Liquid Crystals Science and Technology Section A: Molecular Crystals and Liquid Crystals* **334** 477
[191] Bramwell S T and Holdsworth P C W 1993 *J. Phys.: Cond. Mat.* **5** L53
[192] F.Palacio F et al. 1997 *Phys. Rev. Lett.* **79** 2336
[193] Pratt F L et al. 2000 *Physica. B* **289** 119
[194] Reis A H et al. 1979 *J. Am. Chem. Soc.* **101** 2756
[195] Miller J S et al. 1979 *J. Am. Chem. Soc.* **101** 7111
[196] Candela G A et al. 1979 *J. Am. Chem. Soc.* **101** 2755
[197] Clerac R et al. 2003 *Chem. Mater.* **15** 1840
[198] Berlie A et al. 2013 *J. Appl. Phys.* **113** 17E304
[199] Chittipeddi S et al. 1997 *Phys. Rev. Lett.* **58** 2695
[200] Uemura Y J et al. 1994 *Hyp. Int.* **85** 133
[201] Kurmoo M 1998 *New J. Chem.* **22** 1515
[202] Manson J L et al. 1998 *Chem. Mater.* **10** 2552
[203] Batten S R et al. 1998 *Chem. Comm.* **10** 439
[204] Steele A J et al. 2011 *Phys. Rev. B* **84** 064412

[205] Manousakis E 1991 *Rev. Mod. Phys.* **63** 1
[206] Lancaster T et al. 2006 *Physica. B* **374-375** 118
[207] Baker P J et al. 2010 *Phys. Rev. B* **82** 012407
[208] Hu K L et al 2009 *Chem. Eur. J.* **15** 12050
[209] Wang X Y 2004 et al. *Inorg. Chem.* **43** 4615
[210] Satija S K et al. 1980 *Phys. Rev. B* **21** 2001
[211] Ishida T et al. 2009 *Inorg. Chem.* **48** 7012
[212] Branzoli F et al. 2010 *Phys. Rev. B* **82** 124401
[213] Salmon Z et al. 2010 *Phys. Rev. B* **82** 174427
[214] Drew A J, Szulczewski G, Nuccio L and Gillin W P 2013 *Phys. Stat. Sol. B*, **249** 9
[215] Dediu V A et al. 2009 *Nat. Mat.* **8** 707
[216] Petkov V et al. 2002 *J. Am. Chem. Soc.* **127** 8805
[217] Nagamine K et al. 1984 *Phys. Rev. Lett.* **53** 1763
[218] Ishida K et al. 1985 *Phys. Rev. Lett.*, **55** 2009
[219] Nishiyama K et al. 1986 *Hyp. Int.* **32** 55
[220] Pratt F Let al. 1997 *Phys. Rev. Lett.* **79** 2855
[221] Pratt F L et al. 2000 *Physica B*, **289** 625
[222] Blundell S J 2002 *J. Phys.: Cond. Mat.* **14** 9987
[223] Pratt F L 1993 et al. *Synth. Met.* **55** 677
[224] Pratt F L et al. 1990 *Hyp. Int.* **65** 847
[225] Pratt F L et al. 1997 *Synth. Met.* **84** 943
[226] Pratt F L et al. 1997 *Hyp. Int.* **106** 33
[227] Pratt F L et al. 1999 *Synth. Met.* **101** 323
[228] Pratt F L et al. 1995 *Synth. Met.* **69** 231
[229] Pratt F L 2004 *J. Phys.: Cond. Mat.* **16** S4779
[230] Nagamine K et al. 2000 *Physica B* **289** 631
[231] Nagamine K 2002 *Eur. Phys. J. A* **13** 189
[232] Scheicher R H et al. 2003 *Physica. B* **326** 30
[233] Telling M T F and Kilcoyne S H 2012 *Phys. Proc.* **30** 86
[234] Telling M T F and Kilcoyne S H 2007 *J. Phys.: Cond. Mat.* **19** 026221
[235] Torikai E et al. 2001 *Hyp. Int.* **138** 509
[236] Nagamine K and Torikai E 2004 *J. Phys.: Cond. Mat.* **16** S4797
[237] Piroto Duarte J et al. 2010 *Phys. Stat. Sol. C* **7** 996
[238] Piroto Duarte J et al. 2003 *Physica B* **326** 94
[239] Piroto Duarte J et al. 2006 *Phys. Rev. B* **73**, 075209
[240] Piroto Duarte J et al. 2009 *Physica B* **404** 859.
[241] Saragi T P I et al. 2013 *Org. Elec.* **14** 62
[242] I McKenzie 2010 *J. Phys. Chem. A* **114** 12759
[243] Nuccio L et al. 2011 *J. Phys.: Conf. Ser.* **292** 012004
[244] Pramanik S et al. 2007 *Nat. Nano.* **2** 216
[245] Bobbert P A 2010 *Nat. Mat.* **9** 288
[246] Nguyen T D et al. 2010 *Nat. Mat.* **9** 345
[247] Shakya P et al. 2008 *J. Appl. Phys.* **103**, 103715
[248] Pratt F L et al. 2000 *Physica B* **289**, 625
[249] Prokscha T et al. 2005 *Phys. Rev. B* **72** 121401